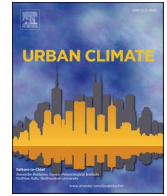




ELSEVIER

Contents lists available at [ScienceDirect](https://www.sciencedirect.com)

Urban Climate

journal homepage: www.elsevier.com/locate/uclim

High-resolution mesoscale simulation of the microclimatic effects of urban development in the past, present, and future Hong Kong

Yu Ting Kwok^{a,*}, Robert Schoetter^b, Cécile de Munck^b, Kevin Ka-Lun Lau^c,
Man Sing Wong^d, Edward Ng^a

^a School of Architecture, The Chinese University of Hong Kong, Hong Kong, China

^b CNRM, Université de Toulouse, Météo-France, Toulouse, France

^c Institute of Future Cities, The Chinese University of Hong Kong, Hong Kong, China

^d Department of Land Surveying and Geo-Informatics, The Hong Kong Polytechnic University, Hong Kong, China

ARTICLE INFO

Keywords:

Urban climate
Urban development
Mesoscale atmospheric model
Urban boundary layer
Urban surface energy balance
Heat stress

ABSTRACT

Anthropogenic modification of the natural environment has caused significant impacts on the local atmosphere and far-reaching changes to the global climate. Taking Hong Kong as a case study, high-resolution (250 m) mesoscale simulations are conducted using Meso-NH coupled with the multi-layer Town Energy Balance to investigate the effects of past (early 1960s), present (2018), and future (late 2040s) urban developments on the city's surface energy balance, heat island, boundary layer structure, and heat stress during a prolonged heatwave event. Overall, horizontal and vertical urban expansion has caused the urban areas to become warmer, drier, less ventilated, and more susceptible to hot nights. The dense built-up urban core in the Kowloon peninsula is also found to deepen the urban boundary layer and enhance the coastal urban heat island circulation. Reclaimed land exhibits the largest differences in 2-m air temperature relative to a no urban scenario due to the drastic change in surface thermal properties. Areas downwind of the planned artificial islands in East Lantau are expected to experience warmer and calmer conditions due to the altered wind field. Study findings raise awareness regarding the increasingly long durations of strong heat stress in urban areas and the need for heat stress mitigation.

1. Introduction

Hong Kong, now an international financial hub, experienced rapid urbanization since the start of its British colonial era in 1841. From a humble fishing village, the city flourished in trade and light industries in the mid-19th century, and then further transformed into the current metropolis known for its high-density, high-rise developments (Shelton et al., 2011) (Fig. 1). However, the city's spectacular urban settings and success in economic growth were accompanied by marked changes in its local climate conditions. The Hong Kong Observatory recorded an increase of 0.12 K/decade in annual mean temperature at its headquarters (station HKO in Fig. 2b) between 1885 and 2008, during which the rate of increase accelerated to 0.27 K/decade in the last three decades (Ginn et al., 2010). Background climate change is found to have contributed around 40–50% of the observed warming trend, while the rest is likely due to local urbanization, in particular the reduction of greenery coverage, development of new towns, and extensive reclamation in coastal urban areas (Chan et al., 2012; Lau and Ng, 2013). A clear anthropogenic influence was also reflected by the reduction of wind

* Corresponding author.

E-mail address: ytkwok@link.cuhk.edu.hk (Y.T. Kwok).

<https://doi.org/10.1016/j.uclim.2021.100850>

Received 23 January 2021; Received in revised form 2 April 2021; Accepted 13 April 2021

2212-0955/© 2021 Elsevier B.V. All rights reserved.

speed with a rate of -0.60 m/s per decade at the urban station King's Park (station KP in Fig. 2b) from 1968 to 1995, which continued at a reduced rate of -0.16 m/s per decade even after its relocation to higher grounds (Ginn et al., 2010; Peng et al., 2018). Moreover, a ten-fold increase in the occurrence of reduced visibility (below 8 km as observed from station HKO), particularly in winter and spring, was observed in the same period due to particulate pollution from local human activities and, more importantly, pollutants carried by the northeast monsoon from other fast-developing cities in the Pearl River Delta (PRD) region like Shenzhen and Guangzhou (So et al., 2007; Ginn et al., 2010).

At a larger scale, there have been statistically significant changes in various extreme weather conditions in Hong Kong owing to climate change. The probability of a daily maximum temperature (T_{\max}) ≥ 35 °C increased more than seven-fold in the early 21st century compared to the early 20th century (HKEB, 2015). The annual numbers of very hot days ($T_{\max} \geq 33$ °C) and hot nights (daily minimum temperature $T_{\min} \geq 28$ °C) rose while the annual number of cold days ($T_{\min} \leq 12$ °C) dropped; these trends are projected to continue, with more than 150 hot nights per year expected by the end of the century for a high emission scenario (i.e. RCP8.5) (Wong et al., 2011; Shun and Lee, 2017). In the last few decades, heatwaves affecting the PRD region have also become more frequent, intense, and prolonged, and such rising trends were observed to be more prominent in highly urbanized areas (Luo and Lau, 2017). Hot weather was often compounded by dry spells of increased length during summer, with abrupt occurrences of extreme rainfall that may have been intensified by urban thermal perturbations (Wong et al., 2011; Wu et al., 2019).

Apart from analysing past observations, the effects of urbanization on the local atmosphere and surface energy balance (SEB) are commonly quantified using mesoscale atmospheric model simulations (Kwok and Ng, 2021). Numerous numerical studies have been conducted to better understand the climatic influence of past urbanization, as well as to assess the potential impacts of climate change and future urbanization in the PRD region. Earlier studies by Lin et al. (2007, 2009) employed the fifth-generation NCAR/PSU Mesoscale Model (MM5) and a land surface model with bulk urban representation to simulate at 3 km spatial resolution the regional climatic variations caused by land cover changes detected from satellite images of the 1970s and 2000s. Mean monthly near-surface air temperature, sensible heat flux (Q_h), and planetary boundary layer (PBL) height were found to have increased, while mean monthly near-surface relative humidity, mixing ratio, and latent heat flux (Q_e) have decreased in both wet summer and dry autumn conditions.



Fig. 1. Photo overlooking the two sides of Victoria Harbour from the Peak in Hong Kong Island showing urban developments in (a) 1962 (HKLandsD, 2013) and (b) 2020.

Using the Weather Research and Forecasting (WRF) model coupled to a single-layer urban canopy model (UCM), Wang et al. (2014) concurred with similar findings, and noted also a general reduction in wind speed and increased occurrences of short-lived, heavy rainfall. Urban surface data with improved precision (low-rise, mid-rise, high-rise urban categories) were made available by the World Urban Database and Access Portal Tools (WUDAPT) initiative (Ching et al., 2018), allowing Tse et al. (2018) to obtain a more spatially refined (1 km resolution) understanding of the urban-induced differences in meteorological variables between 1988 and 2010, including a local strengthening of sea breezes in coastal urban areas of the PRD region. In the above studies, simulations were conducted using the same initial and boundary conditions with different land cover datasets to isolate the effects of urbanization and the associated alterations in surface energy and momentum exchanges. Their results indicate a modification of the local climate that can be expected given the increasing urbanization.

Taking into account the future climate conditions (RCP8.5) for 2030, Wang et al. (2019c) projected using WRF-UCM a ~ 0.2 K increase in 2-m temperature and a 5–10% increase in probability of extreme heat stress due to climate change alone in the PRD region with reference to the conditions in 2010. Considering also the projected future urban expansion based on past trends, the rise in summer 2-m temperature can go up to 2 K under the same initial and boundary conditions (RCP8.5 for 2030) (Yeung et al., 2020). 10-m wind speed of inland urban areas is projected to decrease by ~ 1 m/s and heat stress falling into the ‘danger’ category (wet-bulb globe temperature ≥ 31 °C) is expected throughout the day (Yeung et al., 2020). Such findings provide the important scientific basis for local governments to conduct future city planning and to formulate the necessary actions to reduce heat-health risks. However, previous regional-scale studies often lack precision in the satellite-derived or projected urban land cover inputs and thus fail to represent the spatial variability of model outputs for practical uses within individual cities.

The Hong Kong Government has set out a long-term strategic plan which emphasizes the enhancement of the city’s liveability and sustainability by incorporating climate-responsive urban planning (HKDB and HKPlanD, 2016). It would therefore be useful to examine how the different ways adopted to develop the city (e.g. coastal reclamation, new town development, urban densification) have influenced the urban climate. The potential effects of future urban (re)developments in Hong Kong also need to be assessed so that timely recommendations may be offered to relevant stakeholders in the process of retrofitting old building stock and optimising new development areas. As such, the current study employs detailed, bottom-up urban surface data to perform urban climate simulations at high spatial resolution (250 m) for the major urban areas of Hong Kong during a prolonged heatwave event. The main objectives and paper sections are outlined as follows:

- 1) To construct detailed model input maps representing the past, present, and most realistic projected future urban form and function (hereafter PAST, PRESENT, FUTURE, respectively) of Hong Kong (Section 2);
- 2) To set up and evaluate the high-resolution urban climate simulations conducted using the mesoscale atmospheric model Meso-NH coupled to the multi-layer UCM Town Energy Balance (Schoetter et al., 2020) (Section 3);
- 3) To examine the impacts of past, present, and future urban developments on the overall microclimate, urban boundary layer, and heat stress during the simulated extreme hot weather event (Section 4); and
- 4) To highlight the urban climatic effects that have been/may be caused by different local development approaches exemplified in three focus areas and discuss study findings with reference to the literature (Section 5).

Limitations and conclusions of the study, as well as recommendations for further work are presented in Section 6.

2. Past, present, and future urban form and function of Hong Kong

2.1. Overview of the study area

The coastal city of Hong Kong (22.3193° N, 114.1694° E), China has a hilly relief and is unique for its highly heterogeneous natural and urban land covers. It has a subtropical climate with hot and humid summers. Urban development concentrates on the two sides of the Victoria Harbour (Fig. 1) in Kowloon and Hong Kong Island due to historical reasons, and new towns are later developed in low-lying coastal areas of the New Territories. The main domain of investigation encompasses the major urban centres and three of the most populated new towns in Hong Kong (Fig. 2). This section describes the preparation of model input parameters representing Hong Kong’s urban form and function (parameters on land cover, urban morphology, building characteristics, and human activities) required for mesoscale urban climate simulations (Masson et al., 2020) at three selected points in time – past (early 1960s), present (2018), and future (late 2040s).

2.2. Past urban form and function (PAST)

The PAST represents Hong Kong in the early 1960s (Fig. 1a). Due to the scarcity of flat land suitable for development, compact urban form on central Kowloon and northern Hong Kong Island has already taken shape following two decades of mass migration from the Mainland after the Second World War and the subsequent civil war in China (Zhang, 2000). The Hong Kong Government conducted the first modern Population Census in 1961, tallying just over 3 million residents in the whole territory (CLSO, 1967). This period also marked the beginning of two important urban policies: public housing to provide affordable and safe housing (Smart, 2006) and new town developments to decentralize population from the congested urban areas (Hills and Yeh, 1983), both of which led to rapid horizontal and vertical urban expansion in the 1970s. However, built-up land was still limited to $< 10\%$ of the total land area (CLSO, 1967) and the average building height was only around five storeys (~ 15 m), as restricted by the Building Ordinance in the early 1900s

(Zou, 2013). Few buildings exceeded 40 m, and the tallest building at that time was no more than 90 m (Emporis, 2020). Coincidentally, Hong Kong experienced 9 consecutive very hot days in May 1963 – an extreme hot and dry period which held the records prior to the heat wave in May 2018 selected for this study (Lee, 2018). It would therefore be interesting to ponder what the thermal climate environment had been like in the PAST and how it would differ from the PRESENT when a similar heat wave occurred.

There is relatively good data availability for the early 1960s. As Hong Kong relied heavily on coastal reclamation (mainly along Victoria Harbour) for urban land supply, its coastline changed constantly through time since the mid-19th century. The coastline in 1963 captured from the online interactive map (<http://oldhkphoto.com/coast/Map.html>) is used for the PAST. Territory-wide aerial photography was carried out by Huntings Survey Ltd. in 1964. These aerial photographs allowed the reconstruction of 3D historical building data on the Kowloon Peninsula using a stereo image matching technique (Peng et al., 2017). Other building footprints on inland Kowloon and Hong Kong Island are digitized using the geographic information system (GIS) software ArcMap according to a series of printed maps prepared in 1970 by the Crown Lands and Survey Office. Their corresponding building heights are assigned by conducting a simple geospatial analysis of the reconstructed building data (Peng et al., 2017) according to historical land use (CLSO, 1967), and with reference to old photos (HKLandsD, 2013), and tall buildings recorded in the Emporis building database. Moreover, the 1961 Population Census provides information on the population distribution, economy, and housing at that time (HKCSD, 1969). Air-conditioning use in Hong Kong was uncommon until mid-1970s hence it is assumed that none of the buildings are air-conditioned in the PAST. Data on electricity/gas consumption from the Census and Statistics Department dating back to 1966/1970 are used to approximate internal heat release for residential buildings and mixed commercial-residential shophouses ('Tong Lau') in the PAST. It is assumed that the construction materials for a specific building archetype (Table A1) did not change between the PAST and PRESENT. Therefore, other building energy-related parameters are taken to be the same as Kwok et al. (2020). The workflow to obtain model surface input parameters for the PAST is summarized in Fig. A1. Supplementary information on the land use and photos of building archetypes in the PAST can be found in Fig. A2.

2.3. Present urban form and function (PRESENT)

Present-day Hong Kong is characterized by a compact high-rise urban environment (Fig. 1b) which occupies only a quarter of the territory's total land area (HKPlanD, 2020). The most recent Population By-census (conducted in 2016) yields a resident population of 7.34 million, more than two times of that in 1961 (HKCSD, 2018). With more than 10,000 high-rise buildings (height 35–100 m) and 3000 skyscrapers (height > 100 m), Hong Kong currently holds the title of the tallest city in the world (Emporis, 2020). Although deep street canyons and bulky podium-and-tower structures are prevalent in the old and new urban areas of Hong Kong, the fraction of pervious surface provided by urban parks is relatively high compared to typical compact urban settings in other parts of the world (Kwok et al., 2020). The most common building use is governmental/communal facilities, followed by residential (Table A1). Within the domain of investigation, commercial activities concentrate along the two sides of the Victoria Harbour, while light industrial activities are dispersed in the new towns in the New Territories. The detailed method of constructing the PRESENT urban form and function based on administrative building and road data, satellite-derived vegetation cover, a survey on building construction practices, and an inventory of electricity and gas consumption is given by Kwok et al. (2020). Model results for the PRESENT are evaluated against observations from surface stations and radiosoundings for the selected study period (Section 3.3).

2.4. Future urban form and function (FUTURE)

The FUTURE scenario assumes the most likely demographic projection and that current urban development plans are put into action. It represents a 'business-as-usual' scenario which shall serve as the baseline in subsequent studies where the effects of potential changes in urban form, building construction practices, and building energy use (e.g. ventilation corridors, district cooling systems, more responsible air-conditioning use) on the urban climate will be investigated. The FUTURE is constructed based on the PRESENT, with the addition of new developments planned within the next 30 years, as well as the planned and potential redevelopment of older urban areas. Hong Kong is facing a shortage of land supply to accommodate the increasing population, projected to peak at around 8.2 million in 2043, and the corresponding demands for housing, offices, and urban infrastructures (HKDB and HKPlanD, 2016). Apart from recovering land from old quarries/mines (e.g. Anderson Road Quarry, Cha Kwo Ling Kaolin Mine), developing the vacant site at Kai Tak Airport which ceased operation in 1998, and tapping into brownfield sites in the New Territories, reclamation remains as a main strategy for land supply in Hong Kong. In the 2018 Policy Address, the Government proposed a controversial project to reclaim 1700 ha of artificial islands and develop the East Lantau Metropolis (ELM; Fig. 2c) (HKSAR, 2018), a project now named as Lantau Tomorrow Vision. The designated task force on land supply also recommended five near-shore reclamation sites outside the Victoria Harbour, including three within the domain of investigation, to serve as medium- to long-term options. Major new development areas are outlined in Fig. 3c. Surface cover, urban morphology, and building use in these areas are constructed based on publicly available development plans (Table A2). Since no drastic changes in the socioeconomic activities of Hong Kong are expected in the next few decades, the range of building archetypes and their associated building use, material properties, and occupant behaviours are thus assumed to be the same as for the PRESENT, with the exception of an implementation of the first district cooling system (DCS) in Hong Kong for non-domestic buildings in the Kai Tak new development area in East Kowloon. In the model, the DCS is set with a higher rated coefficient of performance and the waste heat and moisture from air-conditioning is not released into the atmosphere.

The problem of ageing building stock in Hong Kong, particularly in central Kowloon, is expected to intensify in the next decades. If no buildings are demolished, there will be more than 300,000 private housing units and 24 public housing estates over 70 years old by 2046 (HKDB and HKPlanD, 2016). To emulate redevelopment in the model input maps, building data at 32 sites are updated in

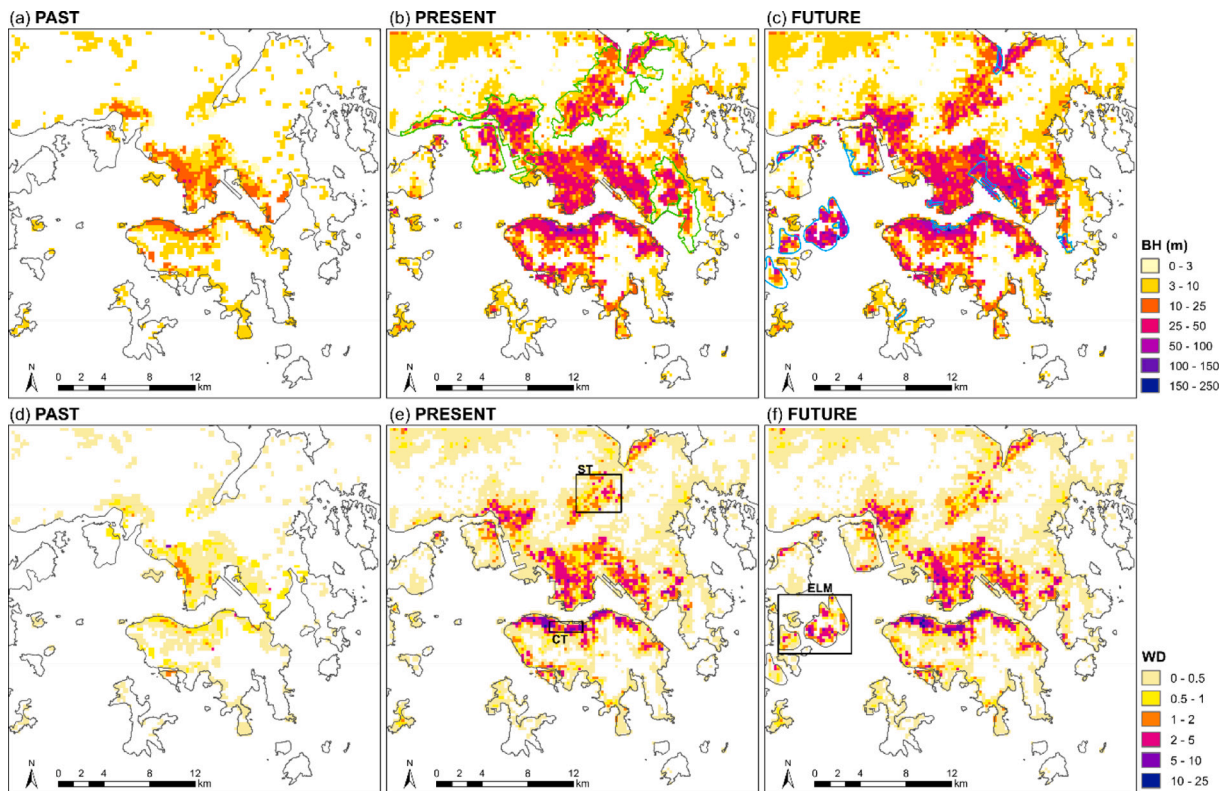


Fig. 3. Building height and wall density (vertical external façade area/horizontal grid area) for the (a,d) PAST, (b,e) PRESENT, and (c,f) FUTURE within the domain of investigation. New towns (green) are outlined in (b) and the major new development areas (blue) are outlined in (c). The selected subdomains for discussion in Section 5.1 are marked and labelled in (e) and (f). The difference in building height and wall density for PRESENT-PAST and FUTURE-PRESENT are shown in Fig. A3 in the Appendix. (For interpretation of the references to colour in this figure legend, the reader is referred to the web version of this article.)

accordance with the project plans listed by the Urban Renewal Authority (URA, 2020) and restrictions set out in the Outline Zoning Plans (OZP) (TPB, 2020). With reference to the proportion of old buildings, past trends, and building stock studies in other countries (Artola et al., 2016), building redevelopment rates of 0.125–1%/year are assumed for different districts in Hong Kong. The implementation in a GIS involves a change in building archetype (from ‘Old commercial building’ to ‘Commercial skyscraper’, from ‘Tong lau’/‘Private housing’ to ‘Newer Private housing’, from ‘Informal infrastructures’ to ‘Other GIC’; Table A1), an increase of building height up to the maximum allowed for the zone (TPB, 2020), and a reduction of building footprint to increase public open space (HKDB and HKPlanD, 2016) at randomly selected building sites of the PRESENT. Furthermore, the Government has been encouraging the revitalization of industrial buildings to commercial offices in East Kowloon since 2010. This process is assumed to continue, but at a reduced rate of two buildings per year in the next 30 years due to strata ownership issues (Wai, 2012).

2.5. No urban land cover (NOURB)

Besides the simulations using the PAST, PRESENT, and FUTURE urban forms and functions, a fourth simulation is conducted with no urban land cover. Oke (2006) pointed out the importance of being able to isolate the climatic modifications due to urban developments based on Lowry’s framework for estimating urban climate effects (Lowry, 1977). Since there is likely already a considerable urban effect by the developments existing in the PAST, NOURB is created to serve as a baseline. The NOURB is constructed by replacing all grids and grid fractions with a town land cover in the PAST by a nature land cover (Fig. 2a), specified as ‘Asia wet and dry tropical grassland’ from the Ecosystem Climate Map (ECOCLIMAP-I) database (Champeaux et al., 2005). Empirical studies on the UHI of Hong Kong often suffer from the lack of urban/rural representativeness due to the heterogeneous station environments, significant coastal and orographic influences, and the effects of rapid urbanization in the neighbouring PRD region (Siu and Hart, 2013). Benefiting from the use of numerical simulations to perform ‘controlled experiments’, the urban heat island (UHI) or urban cool island (UCI) in this study shall refer to the air temperature difference between the PAST/PRESENT/FUTURE and NOURB.

3. Model simulation

3.1. Simulation period

A period of extreme hot and dry weather (17–31 May 2018), during which 15 consecutive very hot days and 6 hot nights were recorded at the Hong Kong Observatory, is selected as the simulation period in the current study. This prolonged heat wave is characterized by high air temperature, long sunshine duration, almost no rainfall, and light prevailing winds mainly from the southwest. Due to climate change, such extreme conditions are expected to occur more frequently, and may even become the typical conditions in the future. Extreme heat can lead to severe heat stress (Lee et al., 2016) and increase building cooling demands (Morakinyo et al., 2019). Moreover, a significant association has been found between high temperature and increased mortality risk (Goggins et al., 2012), and the association is even stronger when the high temperature event lasts over a few days (Ho et al., 2017; Wang et al., 2019a). It is therefore crucial to inform decision-makers for public health, urban planning, weather services, and other relevant policies of the potential climatic impacts induced by urban environment and activities during a prolonged heat wave. To eliminate the influences from synoptic weather conditions, the same meteorological conditions are applied to all four simulations with different urban surface and land cover datasets.

3.2. Model configuration

The anelastic nonhydrostatic mesoscale atmospheric model Meso-NH (Lac et al., 2018) is employed to downscale the Integrated Forecasting System high-resolution operational forecast analyses from the European Centre for Medium-Range Weather Forecasts (ECMWF) via three intermediate model domains (D1, 8 km; D2, 2 km; D3, 1 km) to the domain of investigation (D4, 250 m) covering a large part of Hong Kong. A domain with even higher resolution (D5, 125 m) is used to better resolve the complex orography, coastline and urban morphology of Kowloon and Hong Kong Island for model evaluation. The outlines of the model domains and employed physical parametrisations are given in Fig. 2a and Table 1 of Schoetter et al. (2020). The ECMWF analysis data are used to initialize all model domains at 12 UTC of 15 May 2018, and as lateral forcing for D1 during the entire simulation. Two-way grid nesting is applied for D2 to D5. Meso-NH is coupled with the land surface model SURFace EXternalisée (SURFEX; Masson et al., 2013) to solve the surface energy budget as a function of the prevailing meteorological conditions. SURFEX distinguishes four main land cover types, namely sea (Voldoire et al., 2017), water (FLAKE; Salgado and Le Moigne, 2010), nature (ISBA; Noilhan and Planton, 1989), and town (TEB;

Table 1

Comparison of results in D4 for the PAST, PRESENT and FUTURE averaged over the simulated period in May 2018.

Comparison metric	Unit	PAST	PRESENT	FUTURE
Changes in urban areas				
Extent of urban areas (Fig. 2)	grids	1048	2759	3053
Daily mean T2m	°C	29.9(2.06)	30.3 (2.06)	30.3 (2.06)
Daily mean UHI/UCI	K	+0.3 (0.56)	+0.5 (0.73)	+0.5 (0.79)
Daytime mean T2m	°C	32.0 (1.71)	32.4 (1.74)	32.5 (1.75)
Daytime mean UHI/UCI	K	−0.1 (0.49)	+0.3 (0.95)	+0.5 (1.08)
Nighttime mean T2m	°C	28.4 (1.29)	28.7 (1.19)	28.7 (1.22)
Nighttime mean UHI/UCI	K	+0.6 (0.57)	+0.5 (0.67)	+0.5 (0.73)
Daily mean RH2m	%	71.7 (9.03)	69.8 (9.10)	69.5 (8.99)
Difference in daily mean RH2m with NOURB	%	−2.1 (3.19)	−3.2 (3.90)	−3.8 (4.19)
Daytime mean W10m	m/s	3.0 (1.03)	2.6 (1.19)	2.6 (1.18)
Difference in daytime mean W10m with NOURB	m/s	−0.9 (0.82)	−1.3 (1.33)	−1.5 (1.36)
Occurrence of calm wind condition (<0.5 m/s)	grid-hr	20,147	56,118	61,219
Percentage of calm wind occurrence	%	5.34	5.65	5.57
Changes in rural areas				
Extent of rural areas (Fig. 2)	grids	6329	5093	5108
Daily mean T2m	°C	29.0 (2.50)	28.9 (2.52)	29.0 (2.54)
Daytime mean T2m	°C	31.5 (2.19)	31.4 (2.21)	31.4 (2.22)
Nighttime mean T2m	°C	27.3 (1.58)	27.1 (1.58)	27.2 (1.60)
Daily mean RH2m	%	74.1(10.62)	73.9(10.75)	73.6(10.78)
Daytime mean W10m	m/s	3.3 (1.52)	3.2 (1.47)	3.2 (1.45)
Changes in urban heat stress				
Daytime mean UTCI	°C	38.3 (2.93)	38.0 (2.90)	38.0 (2.97)
Evening mean UTCI	°C	31.3 (2.63)	31.6 (2.41)	31.6 (2.42)
Average percentage of time exposed to MHS	%/grid	45.8 (7.58)	44.4 (9.36)	44.4 (9.31)
Average percentage of time exposed to SHS	%/grid	36.7 (8.78)	40.3 (12.8)	44.4 (12.7)
Average percentage of time exposed to VSHS	%/grid	15.6 (6.61)	14.4 (8.11)	14.2 (8.17)
Nighttime mean T2m in residential areas	°C	28.4 (1.30)	28.7 (1.25)	28.7 (1.28)
Mean number of HNHs in residential areas	hr/grid	54 (21.2)	63 (21.7)	65 (21.9)

Standard deviations of averaged metrics are given in brackets. Daytime, evening, and nighttime correspond to LT 11–16, LT 18–21, and LT 1–6. UHI/UCI is defined as the difference in T2m between the PAST/PRESENT/FUTURE and NOURB. Positive and negative differences with NOURB are in red and blue, respectively.

Masson, 2000). The recently developed multi-layer coupling between Meso-NH and SURFEX-TEB (Schoetter et al., 2020) is used to represent the effect of the high-rise buildings in Hong Kong on all atmospheric levels intersecting the buildings. Wind speed reduction due to the drag effect by building walls and roofs, the turbulent kinetic energy production due to wind shear close to buildings, as well as the temperature and moisture increments due to heat and moisture fluxes from building walls and roofs towards the atmosphere are taken into account. A Building Energy Model (BEM; Bueno et al., 2012; Pigeon et al., 2014) solves the energy budget of a representative building at district scale (archetype) as a function of the meteorological conditions, physical characteristics of the building envelope, and human behaviour related to building energy consumption (e.g. internal heat release, air conditioning). Further details about the model configuration are given in sections 3.2 and 3.4 of Schoetter et al. (2020).

With the selected model configuration, the different local climatic influences of the simulated urban development scenarios can be represented. Urban surface datasets for model input in D4 have been described in Sections 2.2–2.5. The resultant extent of urban areas, maps of building height and wall density, and statistical distribution of building archetypes for the PAST, PRESENT, and FUTURE urban forms and functions are shown in Figs. 2 and 3, and Table A1, respectively. The extent of urban areas (grids with dominant town land cover) increased substantially by 1.6 times from the PAST to PRESENT, attributing to significant urban expansion in Kowloon and development of the Shatin, Tsuen Wan, and Tseung Kwan O new towns within D4 (Figs. 2 and 3). There have also been major reclamations along the western coast of Kowloon, northern coast of Hong Kong Island, and within Tide Cove in Shatin, causing a reduction in sea land cover by 5.5%. Between the PRESENT and FUTURE, urban expansion is minimal, except for the new artificial islands in ELM. In terms of building height, buildings are on average few tens of meters taller in the PRESENT than in the PAST, and another few meters taller in the FUTURE than in the PRESENT (Figs. 3 and A3). Changes in wall density largely resemble that of building height, and differences may be explained by the increase of urban open/green spaces in recent developments, resulting in relatively smaller

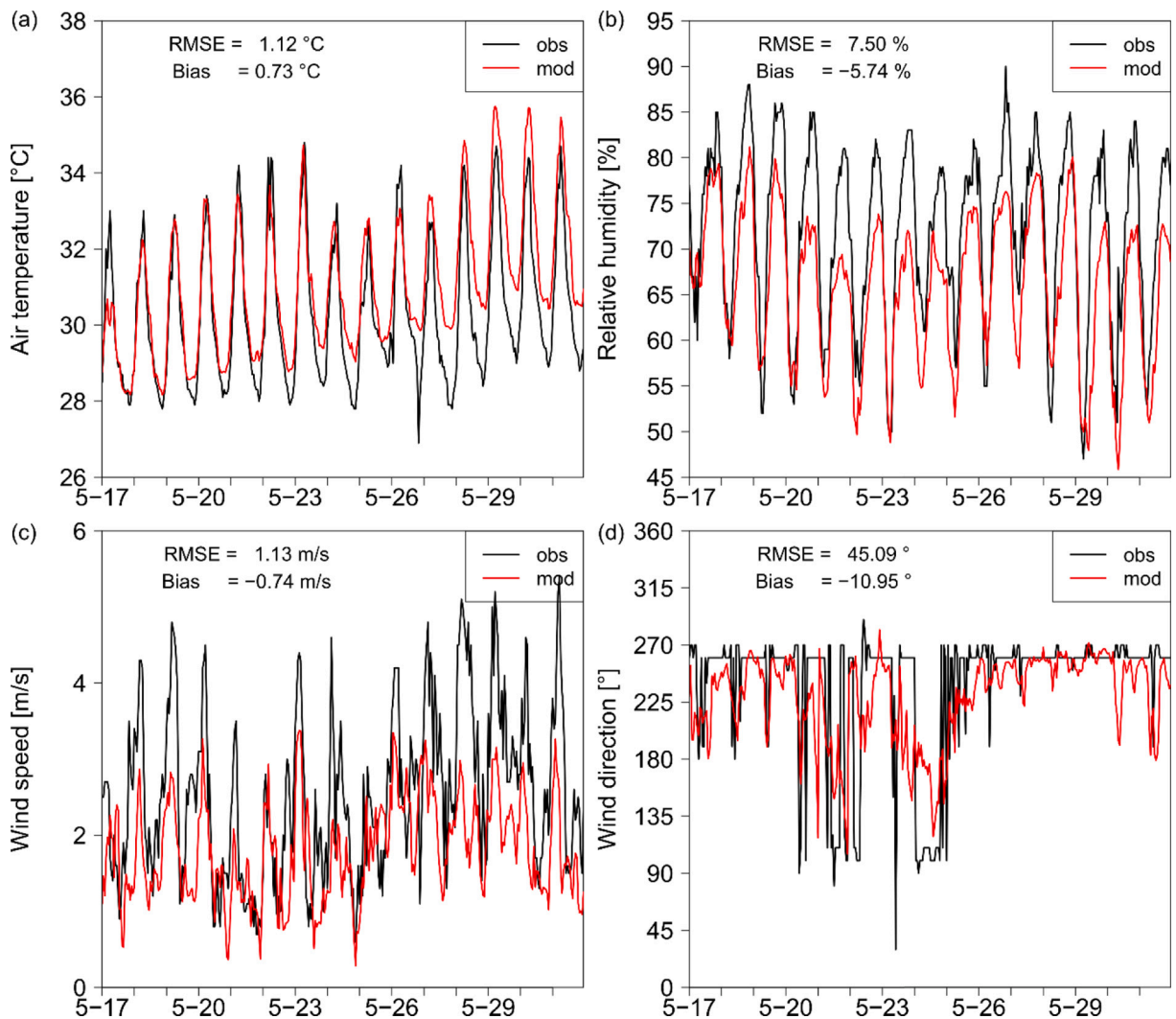
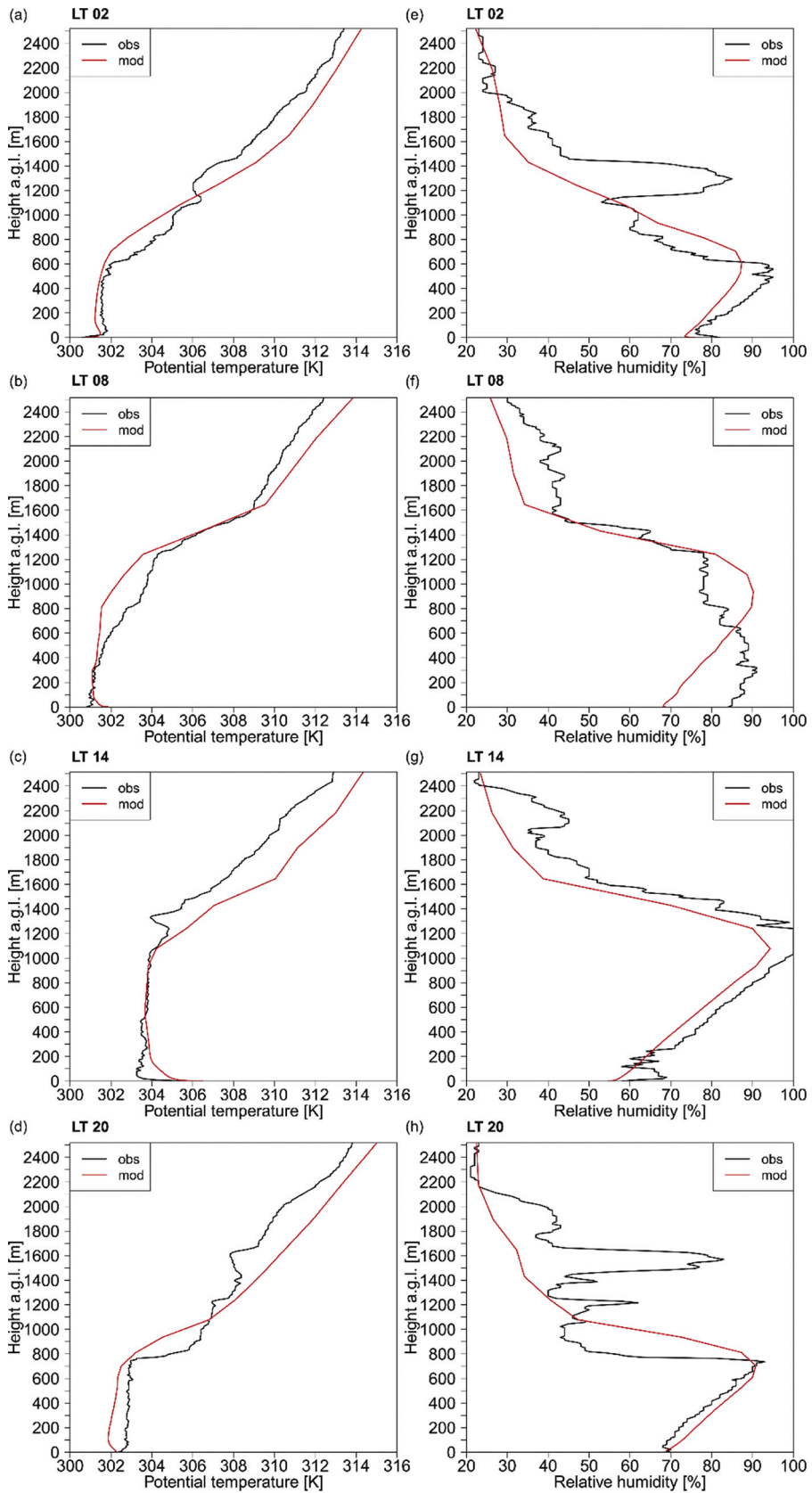


Fig. 4. Time series (UTC) of the modelled (D5) and observed (a) air temperature, (b) relative humidity, (c) wind speed, and (d) wind direction at station HKO during the entire simulated period for the PRESENT.



(caption on next page)

Fig. 5. Vertical profiles of the modelled (D5) and radiosonde observations at station KP of (a-d) potential temperature and (e-h) relative humidity at local time 02 (UTC 18 of the previous day), 08 (UTC 00), 14 (UTC 06), and 20 (UTC 12) on 21 May 2018 for the PRESENT.

increases in built-up density despite the taller buildings. Taller and denser buildings lead to a larger drag force and increased Q_h on more model levels which in turn modify the wind and temperature field. In terms of building characteristics, it is observed from old photographs that buildings are relatively homogeneous in the PAST (Figs. 1 and A2). Since sites with single commercial building use cannot be identified from the available data sources, the number of building archetypes in the PAST is limited to six (Table A1). There are also major differences in internal heat release and air conditioning practices in these archetypes between the PAST and PRESENT/FUTURE. Changes in construction practices lead to changes in the daily cycle of the heat stored in building material, and changes related to the building cooling and energy consumption lead to changes in the anthropogenic heat flux (Q_f). Outside D4, urban input parameters are inferred from a historical local climate zone (LCZ) map of the PRD region in 1978 derived from an early Landsat image using the method of Wang et al. (2019b) for the PAST. Since dramatic urbanization did not take place in the PRD region before the Chinese economic reform in 1978, the use of a 1978 LCZ map to represent the urban form and function in the 1960s is justified. For the PRESENT and FUTURE, urban input parameters beyond D4 are obtained from a locally adapted look-up table based on the PRD LCZ map developed by Cai et al. (2016). Land cover parameters for D1-D2 and all rural areas (nature land cover) are taken from the 1-km resolution global ECOCLIMAP-I database (Champeaux et al., 2005).

3.3. Model evaluation

Model results for air temperature and relative humidity at 1 m above ground level (a.g.l.) and wind speed at the corresponding anemometer heights have been evaluated by Schoetter et al. (2020) for all HKO stations located in D4. There is a slight positive (negative) bias of 0.7 K (−5.3%) for air temperature (relative humidity) averaged over all stations. The root mean square error (RMSE) for air temperature (relative humidity) is 1.2 K (7.6%) and 1.6 K (10.5%) for urban and rural stations, respectively. The wind speed is slightly overestimated with a mean bias (RMSE) of 0.3 m/s (1.2 m/s) and 1.0 m/s (1.8 m/s) for urban and rural stations, respectively. These values indicate a model performance of similar or higher quality than previous mesoscale urban climate simulations in Hong Kong (tables 4 and 5 of Schoetter et al., 2020). The station HKO (Fig. 2b) is considered the most representative of the dense urban environment (Siu and Hart, 2013). It is located on a small elevated (~30 m) park surrounded by high-rise buildings. Even at 125 m resolution, the model grid point closest to the station has a building surface fraction of 0.26 and an average building height of 29 m (Fig. A4). The hourly time series of air temperature, relative humidity, wind speed and direction for station HKO are presented in Fig. 4. Air temperature is well simulated in the first half of the study period, with only a slight overestimation during the night, which may be due to the too-large urban effect in the model grid where the station is located. At the end of the simulation, air temperature is overestimated during both day and night, which may be caused by too-high sea surface temperature. Relative humidity is underestimated during the night, which is consistent with the overestimation of air temperature at this time. The daily cycle of wind speed is not well captured at the station HKO. Wind speed is well simulated during the night, but the model is unable to capture the increase during the day, which is likely due to the channelling of wind from the west into the park by neighbouring buildings. Since the model grid is not free of buildings, the drag force reduces the wind speed too much. The westerly wind direction is well captured.

Vertical profiles of potential temperature (θ), relative humidity, wind speed and direction are evaluated using radiosoundings made at station KP (Fig. 2b) for 21 May 2018 (Figs. 5 and A5). This day is chosen because of the co-existence of sea breeze from the southwest and southeast into the Kowloon peninsula and its clear sky conditions with few low-level clouds. The temperature and wind fields and the boundary layer transition between sea and land will be further analysed for the same day in Section 4. The vertical profiles for θ and relative humidity are captured well, but the amplitude of the daily variation of PBL depth is underestimated since the PBL is too high at Local Time (LT) 02 (about 700 m simulated compared to 600 m observed) but too low at LT 14 (about 1100 m simulated compared to 1300 m observed). Meso-NH also does not simulate the more humid air layers in the region close to the top of the diurnal boundary layer in the evening (LT 20) and night (LT 02). This is likely due to an underestimation of clouds at the top of the boundary layer during the day. Wind speed is considerably underestimated at LT 08, which may be explained by the delayed onset of sea breeze. Wind direction is captured well, except for LT 20 when the wind speed is very low.

4. Results

4.1. Domain-averaged near-surface meteorological variables

Urban and rural areas are defined as the grids in D4 with dominant town and nature land cover, respectively (Fig. 2). The D4-averaged differences in 2-m air temperature (T2m), 2-m relative humidity (RH2m), and 10-m wind speed (W10m) for urban and rural areas for the PAST, PRESENT, and FUTURE averaged over the simulated 15-day heat wave are summarized in Table 1. Overall, larger differences are observed in all variables between the PRESENT and PAST than between the FUTURE and PRESENT, consistent with the changes in urban environment (Figs. 3 and A3). Mean T2m increases slightly by 0.4 K from the PAST to PRESENT/FUTURE in urban areas. The differences in the day (LT 11–16) and night (LT 1–6) are similar. When comparing PAST to NOURB, there is a daytime UCI of 0.1 K and nighttime UHI of 0.6 K. This is probably due to the dominant effect of increased shading and heat stored in the day and subsequently released at night by buildings (Section 4.2). The mean UHI is around 0.5 K for the PRESENT and FUTURE throughout the day. Meanwhile, mean RH2m is slightly (~2%) lower in the PRESENT/FUTURE than in the PAST, which is coherent with the

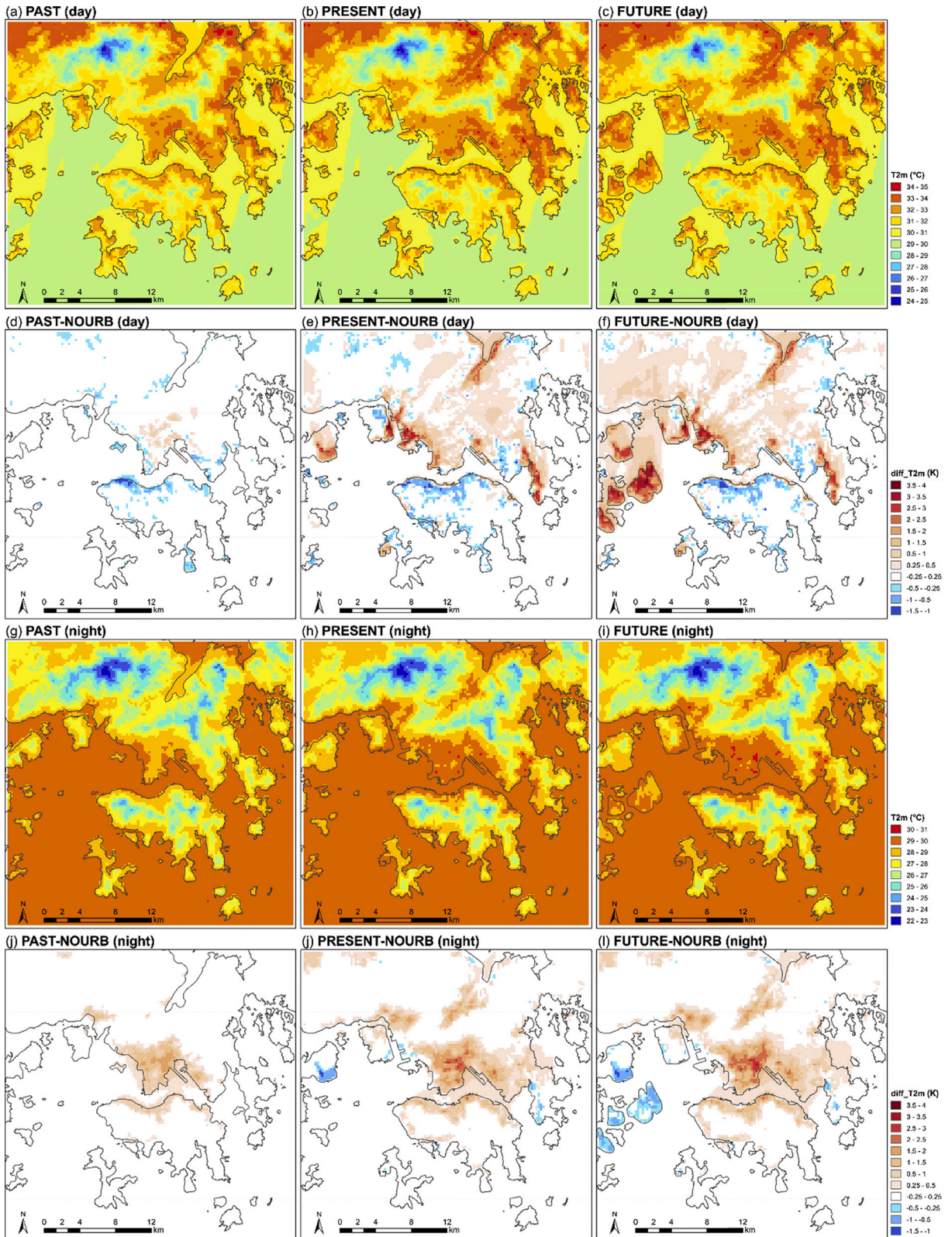


Fig. 6. Mean (a,b,c) daytime (LT 11–16) and (g,h,i) nighttime (LT 1–6) 2-m air temperature for the PAST, PRESENT, and FUTURE and the difference in mean (d,e,f) daytime and (j,k,l) nighttime 2-m air temperature relative to NOURB in the simulated period within D4.

differences found for T2m when considering the Clausius-Clapeyron relation. The decrease in mean daytime W10m by 0.4 m/s from the PAST to PRESENT/FUTURE is considerable (~15%) given the low wind speed during the simulated period. This is a result of the increased drag force due to the higher and denser buildings in the PRESENT/FUTURE relative to PAST (Fig. 3). The reduction in mean urban W10m is even greater when compared to NOURB, ranging from 0.9 m/s for the PAST to 1.5 m/s for the FUTURE. The mean nighttime W10m is generally low (<1.5 m/s) during the simulated period in urban areas; it is therefore not reported in Table 1. Instead, the occurrence of calm wind (<0.5 m/s according to the Beaufort scale) conditions in urban areas is analysed. Calm wind occurs in around 5.34–5.65% of all urban areas and hours of the simulated period for the PAST, PRESENT, and FUTURE. However, due to the increase in the number of urban grids, it translates to an almost three-fold increase in spatial coverage of calm wind conditions from the PAST to PRESENT/FUTURE. In rural areas, the simulated meteorological conditions are largely similar despite the changes in urban development.

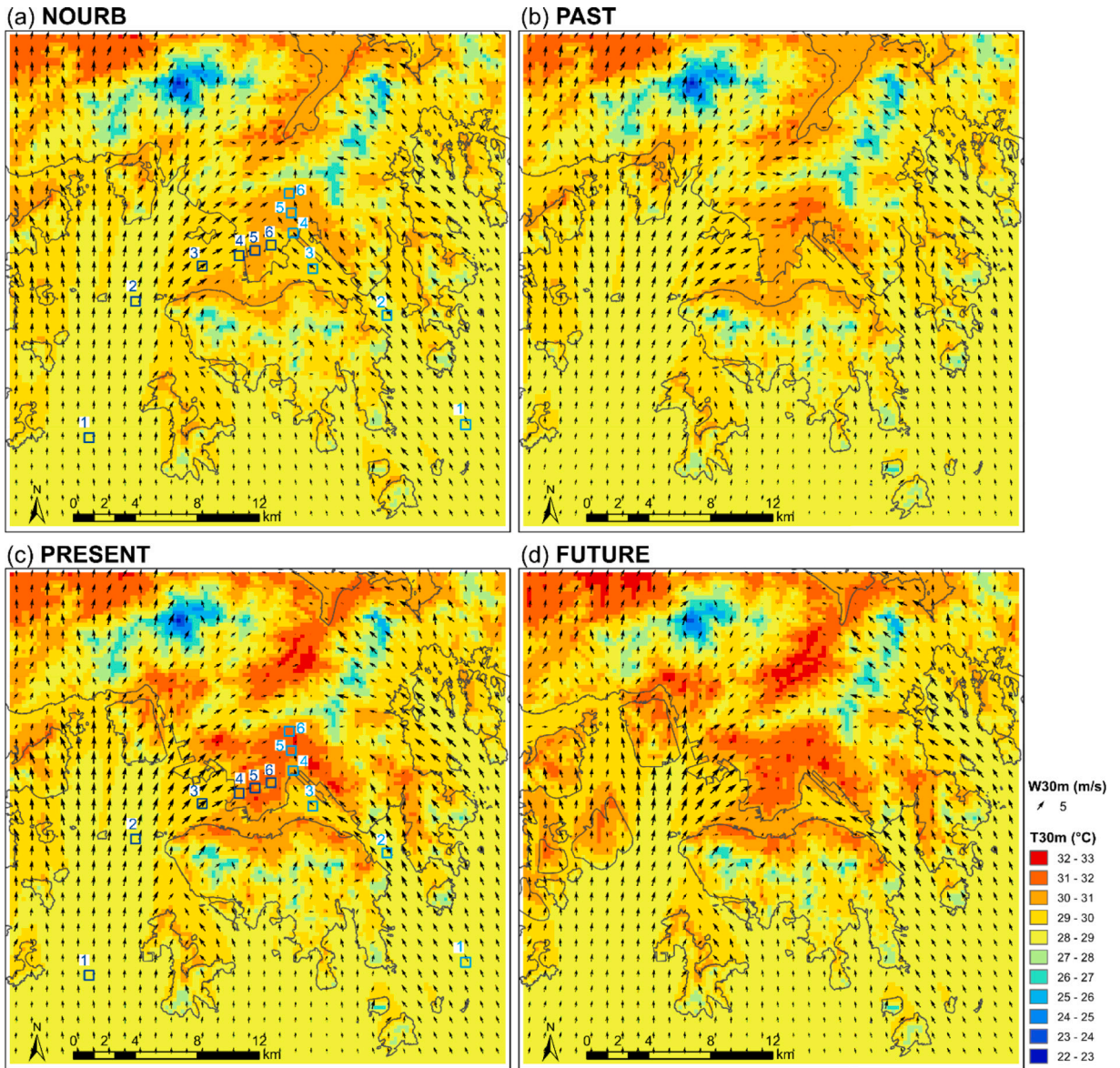


Fig. 7. Mean wind field and air temperature at 30 m above ground level in the daytime (LT 11–16) for (a) NOURB, (b) PAST, (c) PRESENT, and (d) FUTURE on 21 May 2018 within D4. Locations of averaged (2×2 grids) vertical profiles shown in Figs. 9 and 10 along the south-westerly (SW1–6) and south-easterly (SE1–6) wind flows are marked in dark blue and light blue, respectively, in (a) and (c). The location of SW5 coincides with station KP, where evaluations are shown in Figs. 5 and A5. (For interpretation of the references to colour in this figure legend, the reader is referred to the web version of this article.)

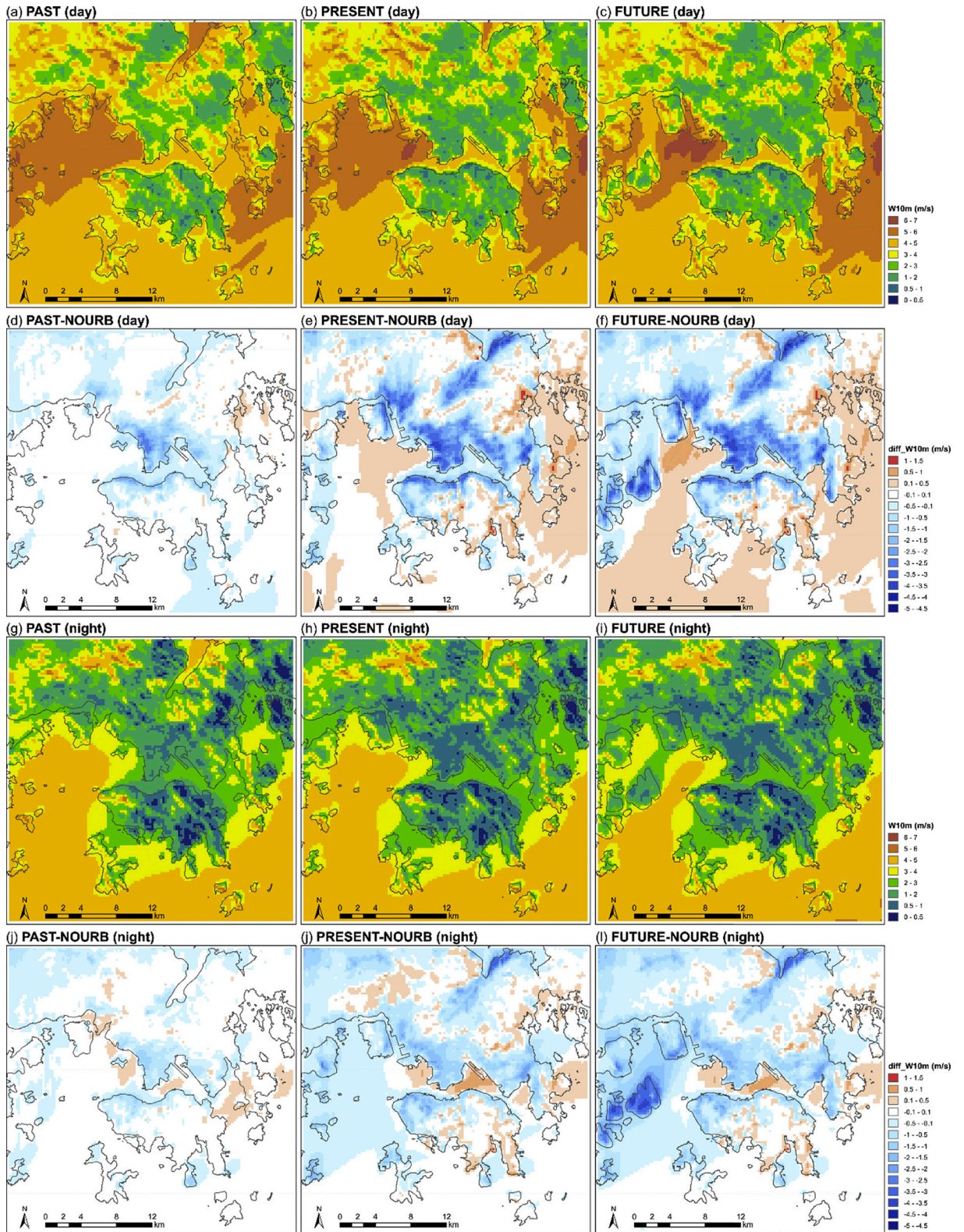


Fig. 8. Same as Fig. 6 but for 10-m wind speed.

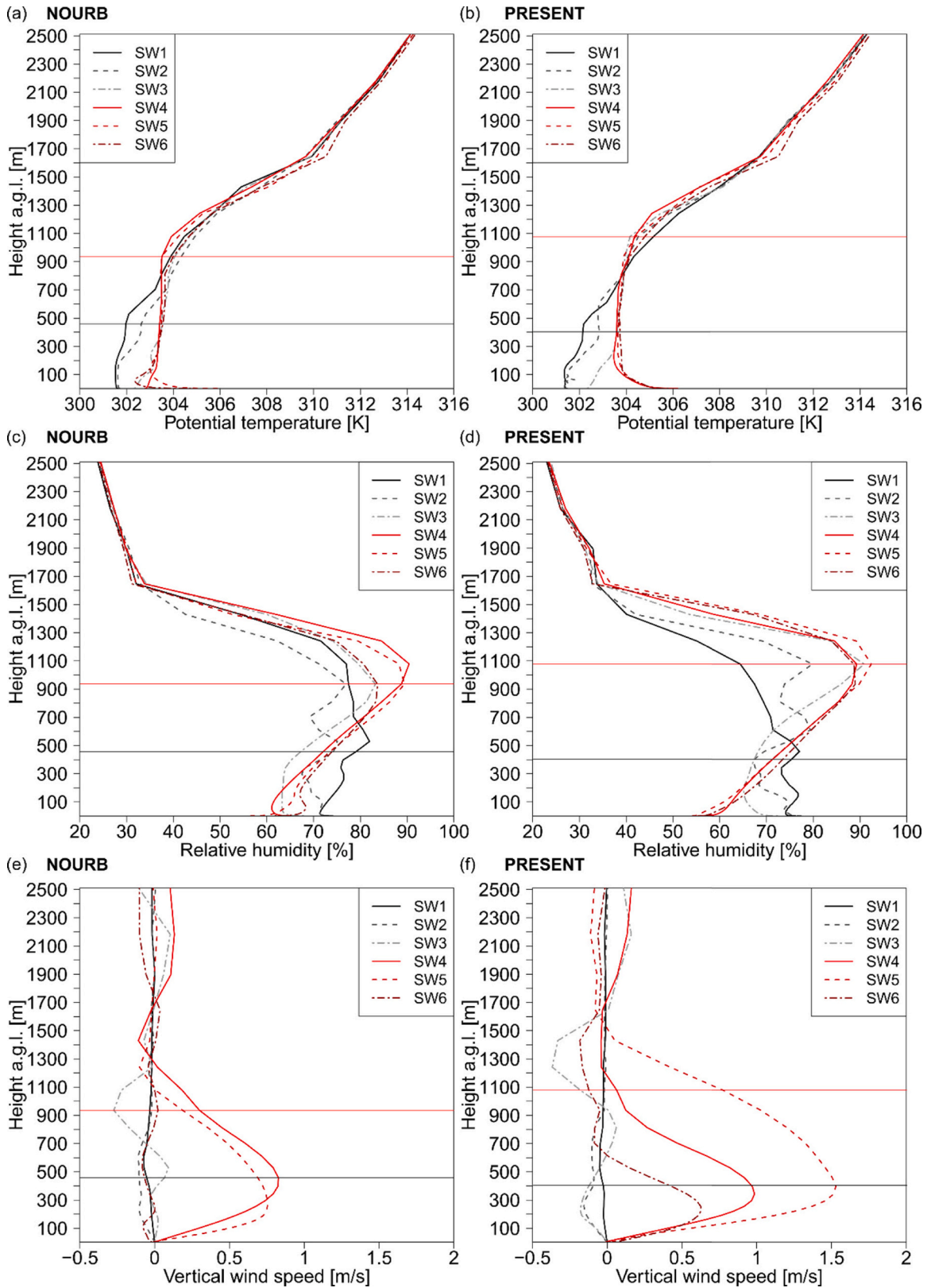


Fig. 9. Vertical profiles of (a,b) potential temperature, (c,d) relative humidity, and (e,f) vertical wind speed along the transect following the south-westerly wind flow (SW1–6) shown in Fig. 7 for NOURB and PRESENT on 21 May 2018 at LT 14 (UTC 06). Vertical profiles over the sea and land are

shown in black/grey and red, respectively. The planetary boundary layer depth of profiles 1 and 4 for both scenarios are estimated from potential temperature based on Sullivan et al., 1998. (For interpretation of the references to colour in this figure legend, the reader is referred to the web version of this article.)

4.2. Spatial variation in near-surface air temperature and wind

Local topography as well as urban surface morphology and land use have been identified as influential factors of the urban climate in Hong Kong (Shi et al., 2019); the focus of this study is on the latter. Since the changes in urban land cover involve a complex interplay of several processes, including reclamation, urban expansion to suburban/rural areas, and intensification of developments in existing urban areas, the statistics presented in Section 4.1 can only provide an overall comparison, but fail to capture the spatial heterogeneity of the differences of the simulated meteorological variables between NOURB, PAST, PRESENT, and FUTURE. Referring to Fig. 6a–c, daytime hot spots coincide with low-lying urban areas, which expanded markedly from PAST to PRESENT and FUTURE. Due to the cooling effect brought by the westerly sea breeze that develops on most days during the simulated period (Fig. 7), the eastern part of Kowloon is on average warmer than the western part. When compared with NOURB, a mean UCI of up to 1.5 K is found in the north-western coast of Hong Kong Island for PAST, PRESENT, and FUTURE. In addition to shading by buildings, this may be attributable to the particularly high building density (Fig. 3d–f) in these areas, resulting in high storage heat flux (Q_s) into building materials in the day. The modelled SEB confirms the rapid increase in Q_s in the morning and the much higher building Q_s in the urbanized scenarios (not shown). In the PRESENT (Fig. 6e), daytime UHI has the highest intensity (2.5–3 K) at the Kwai Chung container ports (to the northwest of Kowloon peninsula) and Tseung Kwan O industrial areas (in the eastern part of D4). Two possible reasons for the large T2m difference with NOURB are the change in surface cover properties by reclaiming sea to land (also applies to the western coast of Kowloon and the estuary near Shatin) and the open urban settings on large impervious areas. In the FUTURE (Fig. 6f), the artificial islands in ELM induce a strong daytime UHI of up to 4 K. The heated air is advected downwind to affect areas further north of the ELM (Fig. 7d). At night, a clear UHI can be observed in all the urban areas (Fig. 7j–l). The intensity increases from PAST to FUTURE, reaching a maximum of 3 K in central and eastern Kowloon. As noted by Giridharan et al. (2005), the temporal evolution and spatial distribution of nocturnal UHI correspond to the changes in development extent and urban geometry (Fig. 3). However, reclaimed land is comparatively cooler in the PRESENT and FUTURE than in NOURB owing to the lower heat capacity and faster longwave radiative cooling of land than the original sea. Indeed, the higher relative humidity over the sea leads to higher values of downwelling longwave radiation there and as a consequence a less negative longwave radiation budget over the sea than over the land (not shown).

The wind environment of Hong Kong is also greatly affected by urban developments. There is a considerable reduction of daytime W10m in urban areas; the difference with NOURB increased from around 1–2 m/s in the PAST to 2.5–5 m/s in most areas in the PRESENT and FUTURE (Fig. 8d–f). The changes in wind field can be attributed to the increased surface roughness as urban developments intensify in both building height and density (Fig. 3). The extent of areas experiencing lower wind speed also enlarged as urban areas expanded to the once rural land in the New Territories. The most affected areas are along the coast or on reclaimed land, notably on the western coast of the Kowloon peninsula and Ma On Shan (northeast of Shatin), where the entry of sea breeze is hindered by dense built-up areas (Figs. 3 and 8e,f). Unsurprisingly, the ELM causes a large reduction in W10m up to 4 m/s over the artificial islands and another 1 m/s reduction over the sea downwind during both daytime and nighttime (Fig. 8f,l). The daytime W10m increases over the relatively open seas around Hong Kong Island in the PRESENT and FUTURE (Fig. 8e,f). Increased drag force due to buildings may cause low-level winds to diverge and choose a path with fewer obstacles. Moreover, a channelling effect along the narrow eastern part of Victoria Harbour, facilitated by the taller buildings in East Kowloon in the FUTURE, is observed on some days (Figs. 7d and 8f). At night, the stagnant wind environment over low-lying terrains, with wind speed generally <2 m/s in PAST and <1 m/s in PRESENT/FUTURE, is exacerbated in urban areas, but the difference with respect to NOURB is relatively small (Fig. 8g–l).

4.3. Planetary boundary layer structure

To examine the changes in PBL structure due to the marine-land transition and urban environment, averaged vertical profiles over small selected boxes (Fig. 7a,c) along two transects following the south-westerly (SW1–SW6; Fig. 9) and south-easterly (SE1–SE6; Fig. A6) wind from the sea into Kowloon peninsula are displayed for NOURB and PRESENT. The box SW5 coincides with the location of weather station KP, where the vertical profiles of θ , relative humidity, wind speed and direction have been evaluated against radiosoundings in Section 3.3. 21 May 2018 is chosen for investigation and the profiles at LT 14, when the PBL depth at KP is the largest, are compared. The PBL depths for the profiles SW/SE 1 over the sea and SW/SE 4 over the land, estimated as the height where the increase in θ is the largest based on Sullivan et al. (1998), are marked in the figures. Similar PBL characteristics are observed along the SW and SE transects. For both NOURB and PRESENT, the θ gradient over the sea shows a roughly neutral surface layer which quickly becomes stable at a few hundred m. Over land, θ is generally higher (up to around 800–1000 m) and the PBL is deeper. However, major differences between the NOURB and PRESENT are found over land, suggesting a modification of the meteorological conditions by urban developments on the Kowloon peninsula not only at the surface, but also at higher levels. Taking as an example the vertical profiles SW4–6 (Fig. 9a,b), the urbanized surface is warmer by 1–2 K and an unstable surface layer of around 100 m, which is roughly five times the average building height in the selected boxes, is found. A mixed layer reaching almost 1100 m is present above, and is deeper than that in NOURB by ~150 m. Although the warm and unstable surface layer is less apparent for the profiles SE4–6 (Fig. A6a,b) due to the smaller difference in urban morphology along the transect, a mixed layer ~150 m deeper than in NOURB is also developed. Relative

humidity is slightly lower over the urbanized land surface in PRESENT than in NOURB, but higher at the top of the PBL (Fig. 9c,d). The higher air temperature can explain partly the lower surface relative humidity but cannot explain the higher relative humidity above, where a difference of 2 g/kg in specific humidity is also found (not shown). Therefore, it is speculated that the sea breeze, strengthened by an UHI circulation, draws moisture from the sea and brings it to the top of the PBL by convection, leading to the amplified land-sea difference in relative humidity observed at the PBL top for the PRESENT. This is further supported by the enhanced upwelling over urban areas as shown by the higher positive vertical wind speed within the PBL (Fig. 9e,f).

4.4. Heat stress in urban areas

Heat stress in urban areas is quantified using two indicators: the universal thermal climate index (UTCI) and hot night hours (HNHs) counted as the number of hours with $T_{2m} \geq 28^\circ\text{C}$ during nighttime (Shi et al., 2019). The UTCI is defined as “the air temperature which would produce under reference conditions the same thermal strain as in the actual thermal environment” (Błażejczyk et al., 2010) and is designed to quantify the outdoor thermal comfort experienced by a reference human body using the meteorological variables air temperature, specific humidity, wind speed, and mean radiant temperature. The calculation of the mean radiant

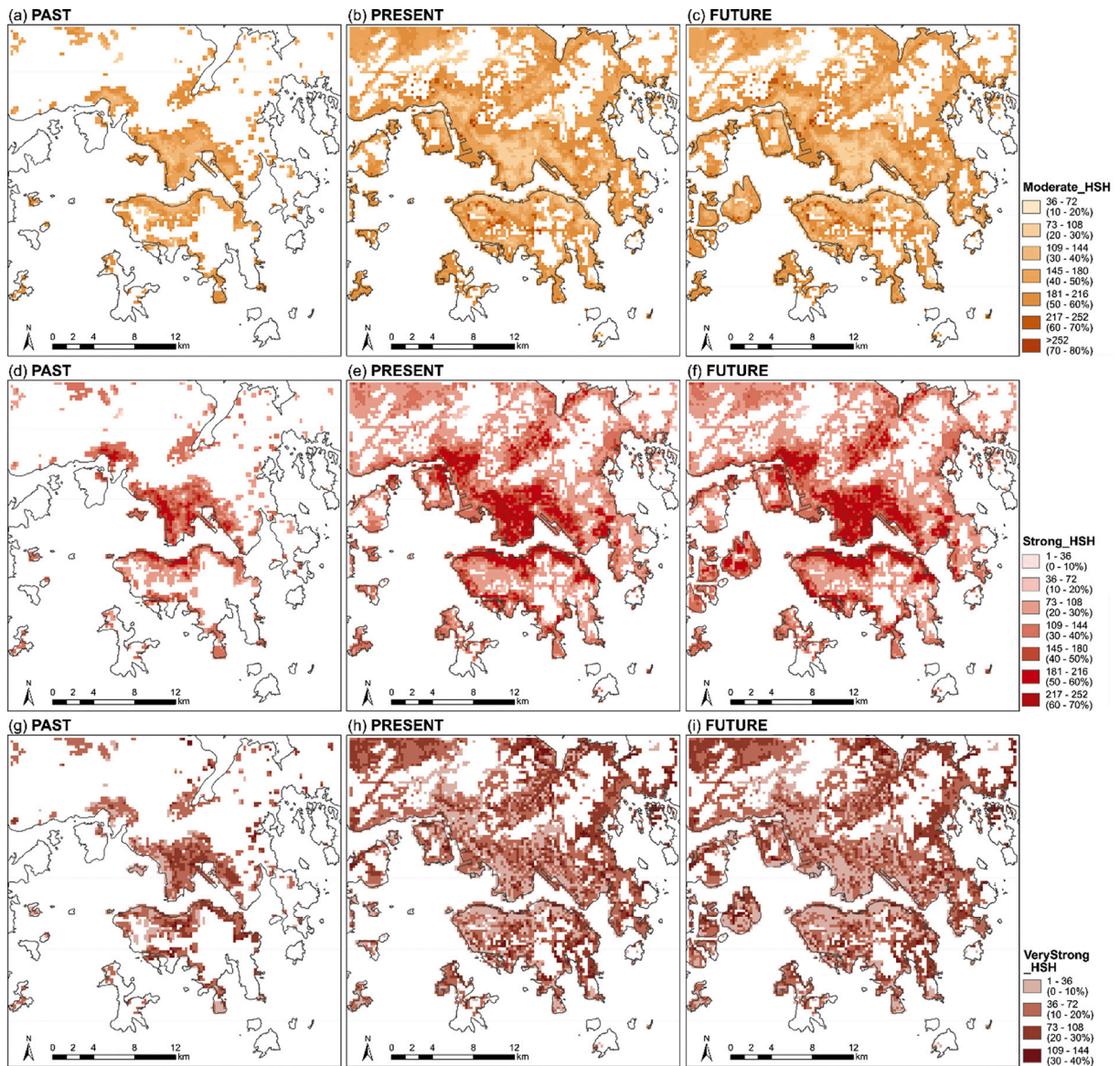


Fig. 10. Number of hours and percentage of time exposed to (a,b,c) moderate heat stress, (d,e,f) strong heat stress, and (g,h,i) very strong heat stress calculated based on the UTCI thermal assessment scale (Błażejczyk et al., 2013) in grids with town land cover for the PAST, PRESENT, and FUTURE during the simulated 15-day (360 h) heatwave in May 2018.

temperature and UTCI in TEB is explained in the Supporting Information of Kwok et al. (2019). Moderate (MHS), strong (SHS), and very strong heat stress (VSHS) are defined by UTCI thresholds of 26 °C, 32 °C, and 38 °C, respectively (Błażejczyk et al., 2013). Since mean radiant temperature is low in the absence of insolation and inhabitants are mostly indoors at night, the UTCI is less suitable for reflecting the nighttime heat exposure of residents, which has been found to cause a more serious health impact than daytime heat exposure (Laaidi et al., 2012; Ho et al., 2017). Therefore, a second indicator with reference to the Hong Kong Observatory’s criterion for a hot night is employed, focusing on residential areas (i.e. urban grids with a dominant residential building use). The number of HNHs averaged per planning district is further compared with the residential population density distribution for the PAST and PRESENT to identify vulnerable districts with high population density and nighttime heat stress.

A simple comparison of the intensity and duration of heat stress in terms of UTCI among the PAST, PRESENT, and FUTURE is included in Table 1. The daytime mean UTCI in urban areas for all three urban form and function is around 38 °C, which corresponds to SHS to VSHS. The mean UTCI remains high (~32 °C) after sunset (LT 18–21), causing MHS to SHS to the urban dwellers. Daytime (evening) UTCI for the PAST is slightly higher (lower) than for the PRESENT and FUTURE. The percentage of time during which heat stress is experienced in the simulated heat wave, normalized per urban grid, is extremely high (Table 1). An increase in the average duration of SHS per urban grid is noted from the PAST to the FUTURE, while the opposite is found for VSHS. Fig. 10 presents the spatial distribution of heat stress in the different categories for the PAST, PRESENT, and FUTURE. There are two key findings: first, SHS to VSHS is experienced in all major urban areas in Hong Kong (Kowloon, northern coast of Hong Kong Island, and new towns) for over 50% of the time during the simulated prolonged heat wave; secondly, shading by dense and tall buildings could mitigate to some extent

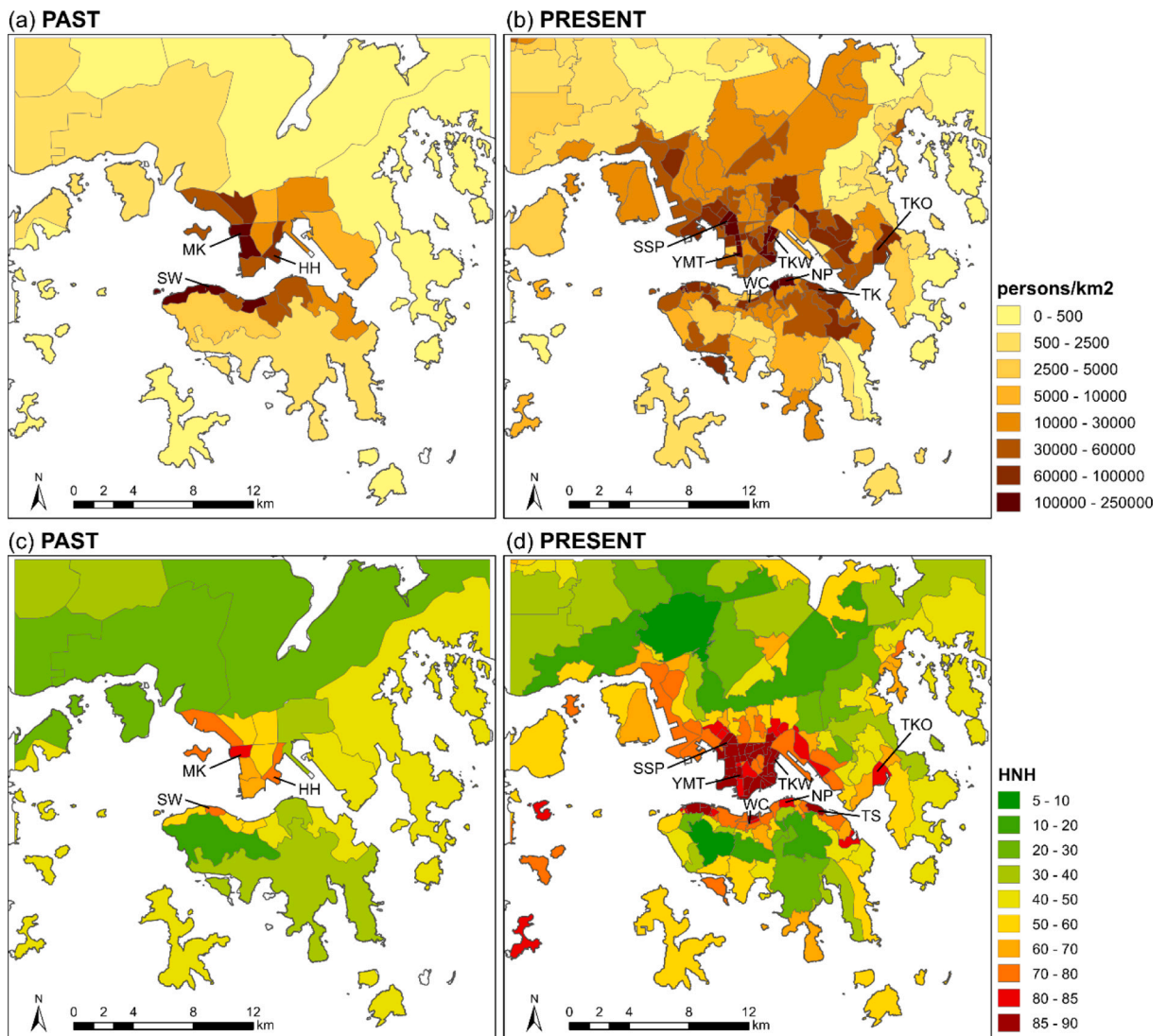


Fig. 11. (a,b) Population density and (c,d) number of hot night hours during the simulated period averaged over planning districts for the PAST and PRESENT. Population data and district boundaries are taken from the 1961 census and 2016 by-census for the PAST and PRESENT, respectively. Vulnerable districts are labelled with acronyms defined in the main text (Section 4.4).

the VSHS, as seen from the relatively lower number of VSHS hours along the western coast of Kowloon in the PAST scenario where building height and density are higher compared to the central and eastern parts (Fig. 3a,d), as well as the reduction in VSHS hours in Kowloon and Hong Kong Island for the PRESENT and FUTURE due to the increase in building height. However, even though dense urban settings may offer opportunities for heat stress relief in the day, the nocturnal UHI in these areas is more pronounced in the PRESENT and FUTURE (Fig. 6j,l).

The mean nighttime T2m in residential areas for the PAST, PRESENT, and FUTURE are all above the hot night threshold of 28 °C (Table 1). Out of the 90 nighttime hours during the simulated period, the mean number of HNHs in residential areas increase from the

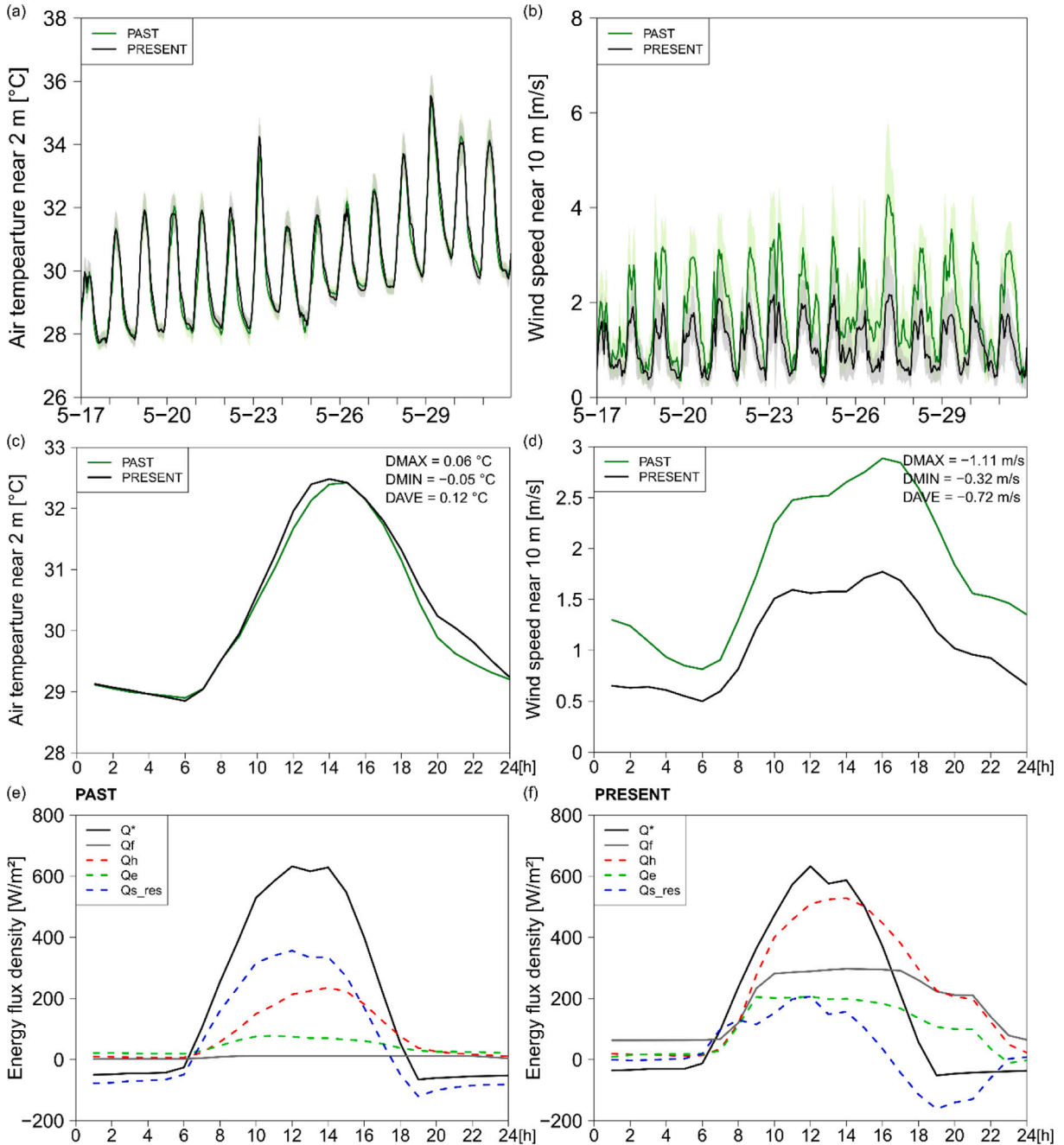


Fig. 12. (a,b) Timeseries (UTC) and (c,d) mean daily cycle (local time) of 2-m air temperature and 10-m wind speed, and (e,f) surface energy balance for focus area CT in the PAST and PRESENT during the simulated period. Metrics shown in (c,d) are obtained by PRESENT-PAST. In the averaged daily cycles, DMAX is the difference in maximum T2m or W10m, DMIN is the difference in minimum T2m or W10m, DAVE is the difference in mean T2m or W10m. In the SEB, Q* is the net radiation, Qf is the anthropogenic heat flux, Qh and Qe are the upwelling turbulent sensible and latent heat fluxes, and Qs_res is the storage heat flux obtained as the residual of other modelled energy fluxes.

PAST (54 h) to PRESENT (63 h) to FUTURE (65 h). As shown in Fig. 11c,d, an average of >80 HNHs is counted for Mong Kok (MK) planning district in the PAST and a majority of planning districts in central Kowloon and a few in northern Hong Kong Island even reach up to 90 HNHs in the PRESENT. Fig. 11 also highlights the vulnerable districts with both high resident population density (>60,000 persons/km²) and elevated nighttime air temperature, including MK, Hung Hom (HH), Sheung Wan (SW) in the PAST, and in addition to these areas, Sham Shui Po (SSP), Yau Ma Tei (YMT), To Kwa Wan (TKW), Wan Chai (WC), North Point (NP), Taikoo Shing (TS), as well as in the Tseung Kwan O (TKO) new town in the PRESENT. The urban heat stress in Hong Kong will be further discussed in Section 5.4.

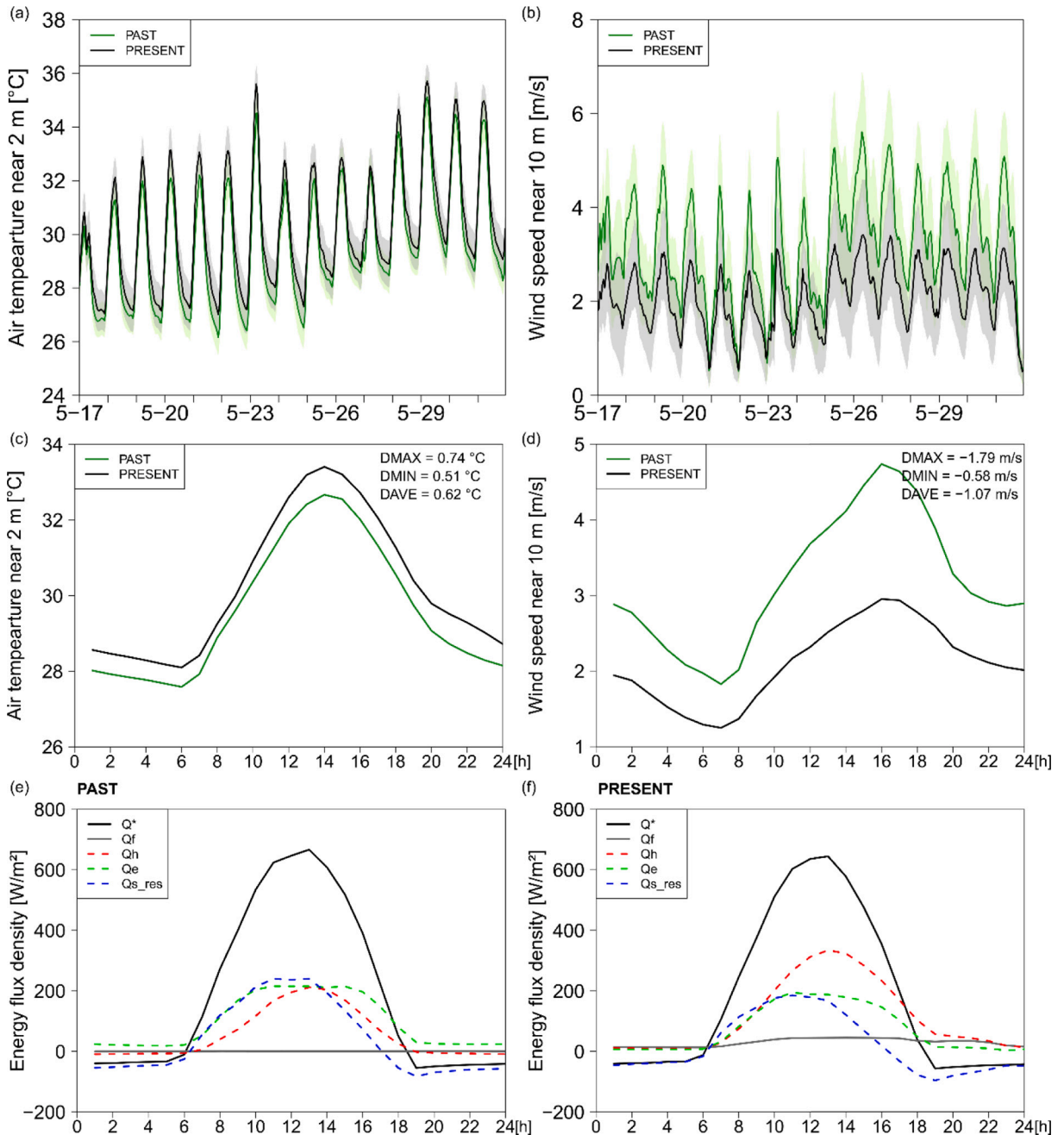


Fig. 13. Same as Fig. 12 but for focus area ST in the PAST and PRESENT.

5. Discussion

5.1. Urban climatic effects of selected urban developments

Three focus areas (Fig. 3e,f), namely Central (CT), Shatin (ST), and the East Lantau Metropolis (ELM), are selected for a more detailed discussion on their changes in urban climate and SEB due to different urban development processes that they have experienced/will experience in the PAST, PRESENT, and FUTURE.

5.1.1. Evolution of the central business district: Central

CT has always been the central business district of Hong Kong. It is the area with the tallest average building height in both PAST and PRESENT (Fig. 3). It also experienced the largest building height increase when old commercial buildings and ‘Tong Lau’ were

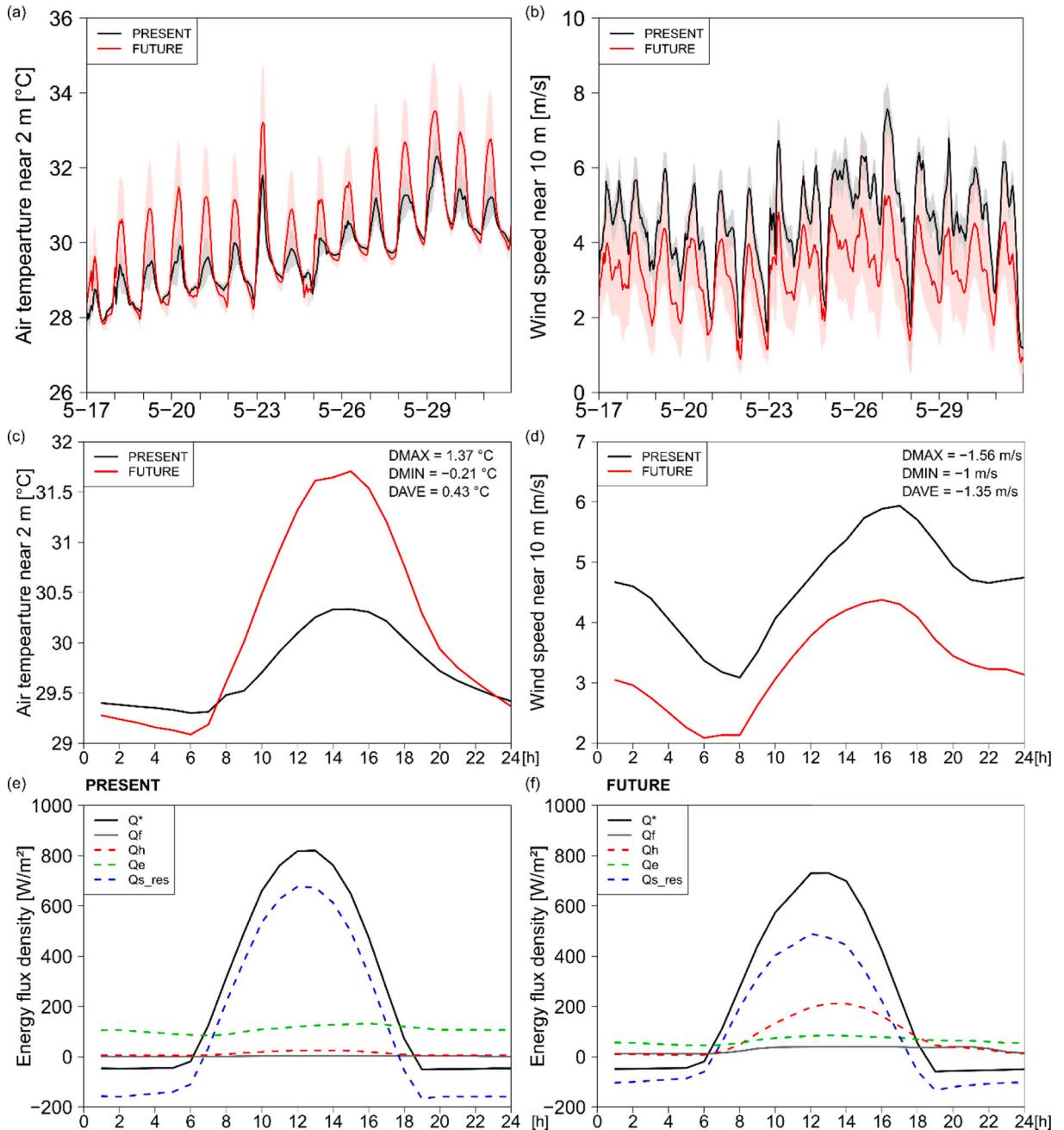


Fig. 14. Same as Fig. 12 but for focus area ELM in the PRESENT and FUTURE. Metrics shown in (c,d) are obtained by FUTURE-PRESENT.

replaced by skyscraping office towers (Fig. A3). In the PRESENT, intensive building energy use and centralized air/water-cooled air-conditioning systems are also introduced, making CT the area with the highest Q_f in Hong Kong (Wong et al., 2015). An analysis of the SEB (Fig. 12e,f) shows a considerable increase in Q_f from a negligible amount in the PAST to $\sim 300 \text{ W/m}^2$ in the PRESENT due to intensive cooling practices during daytime office hours. An accompanying increase in Q_e from ~ 50 to $\sim 200 \text{ W/m}^2$ despite the increased impervious surfaces is likely due to evaporative cooling systems commonly used in new commercial buildings. The cooled building spaces and the building construction materials with lower thermal mass (from mainly concrete to steel frame and glass structures) in the PRESENT may have resulted in lower building Q_s in the day, but Q_s release in the evening has become more rapid and greater in magnitude. Fuelled by anthropogenic heat emissions, Q_h in the PRESENT remains strongly positive in the evening. Surprisingly, the increase in building height and density from PAST to PRESENT has not resulted in a relevant increase in T2m (Fig. 12a,c). In the day, shading by tall buildings may have compensated the increase in thermal load due to higher Q_f and reduced ventilation. In the evening, only a small increase in T2m ($\sim 0.5 \text{ K}$), likely induced by Q_f and the release of heat stored in urban fabric, is found. Another reason for the small difference in T2m may be the multi-layer model structure which distributes the release of anthropogenic heat evenly up to the average building height, as well as the fact that most centralized air-conditioning systems are located on the rooftops. With regards to the urban wind environment, taller buildings in the PRESENT greatly reduce W10m by more than 1 m/s ($>30\%$ of the value for the PAST), especially from noon to late afternoon (Fig. 12b,d).

5.1.2. New town development: Shatin

ST (Figs. 2 and 3) is regarded as one of the first and most successful new towns developed in the 1970s. Its development involved infilling the Tide Cove and Shing Mun River, as well as excavating the nearby hillsides (Hills and Yeh, 1983). The rural villages and farmlands in the PAST have now been transformed into a well-balanced community with a population of almost half a million (HKCSD, 2018). This transformation has inevitably led to considerable changes in the urban climate of ST. The SEB of ST in the PAST resembles a typical suburban area where the Bowen ratio ($\beta = Q_h/Q_e$) is about 1 (Fig. 13e). In the PRESENT, however, Q_h is increased while Q_e is decreased, yielding a β of about 1.5 (Fig. 13f), meaning that more heat is partitioned into the sensible form which makes the lower atmosphere warmer and drier. Compared to the commercial district CT, the mainly residential new town ST produces a much lower Q_f . Q_s is slightly lower in the PRESENT than in the PAST, which could be explained by the reduction of heat uptake by water bodies lost to land reclamation. As shown in Fig. 13c, T2m is $\sim 0.6 \text{ K}$ higher in the PRESENT than in the PAST throughout the day, resulting in more severe heat stress in the day (Fig. 10) and stronger UHI at night (Fig. 6e). The decrease in W10m is particularly large during the day (up to 2 m/s or 40% on some days; Fig. 13b,d) when the potential channelling of wind along the Shing Mun River flowing into Tolo Harbour (Fig. 2) (HKPland, 2012) is hindered by the narrowed river and roughened urban surface.

5.1.3. Large-scale artificial islands: East Lantau Metropolis

To the Government, ELM (Figs. 2 and 3) is a much-needed major development to alleviate the pressing need for land and housing. However, it is met with fierce opposition from the public who worry about the immense environmental and financial costs of the project. The authors therefore feel the need to examine critically the potential urban climatic impacts of the planned artificial islands. As a result of the radical change in surface cover from sea to land, which leads to drastic changes in surface thermal properties (e.g. thermal conductivity, heat capacity, albedo, emissivity), the surface energy fluxes in the PRESENT and FUTURE all differ notably (Fig. 14e,f). The lower net radiation (Q^*) in the FUTURE is likely caused by the higher albedo and emissivity of land and built-up surfaces compared to the sea. The lower heat capacity of the land also leads to less heat storage compared to the sea, resulting in lower Q_s in the FUTURE. And rather expectedly, the warmer and drier land with human activities in the FUTURE contributes to increases in Q_h and Q_f , and a decrease in Q_e .

The daily cycles of T2m over ELM between the FUTURE and PRESENT are markedly different. With a much faster heating and cooling rate on land, the diurnal T2m range in the FUTURE ($\sim 3 \text{ K}$) is around two times that of the PRESENT ($\sim 1.5 \text{ K}$). While being on average $\sim 0.4 \text{ K}$ warmer, the mean maximum (minimum) T2m is $\sim 1.4 \text{ K}$ ($\sim 0.2 \text{ K}$) higher (lower) in the FUTURE than the PRESENT (Fig. 14c). Noting that the focus area ELM incorporates some sea surrounding the islands, an even larger temperature difference reaching 4 K (1 K) is modelled over the hottest (coldest) parts of the artificial islands in the day (at night) (Fig. 6b–c,h–i). Wind speed is reduced by $1\text{--}1.5 \text{ m/s}$ throughout the day owing to the increased surface friction by buildings and vegetation on the islands. It is expected that future inhabitants on ELM would experience long periods of SHS to VSHS, comparable to existing densely-built urban areas, during potential heatwaves such as the one simulated (Fig. 10f,i). Furthermore, the ELM alters the wind field at a larger scale, causing, on the one hand, a convergence downwind (to the north) of the main island, and on the other hand, an acceleration of wind flow to the northeast of the islands in the day (Figs. 7d and 8c). Residents living in areas downwind of the ELM (e.g. Tsing Yi island in the western part of Tsuen Wan new town) may experience calmer winds and warmer conditions, especially under southerly prevailing winds in summer.

5.2. Comparison with previous studies

Several numerical modelling studies have been previously conducted to investigate the climatic effects of urbanization in the PRD region. The modelled mean summer T2m increase due to urbanization over the last three decades ranges from 0.3 K to 2 K , with the smallest values found near the coast and in the already developed areas (e.g. Hong Kong) and the largest in large emerging cities like Guangzhou, Dongguan, Shenzhen, and Foshan (Lin et al., 2009; Wang et al., 2014; Tse et al., 2018). The mean T2m rise of 0.4 K between the PAST and PRESENT therefore matches reasonably well with the previous studies. The two-fold increase in Q_h found for the focus areas CT and ST is also comparable to the findings of Tse et al. (2018), who noted a doubling of Q_h over major urbanized areas in

the PRD region within its first two decades of rapid urbanization. Regarding the wind environment, Wang et al. (2014) modelled a mean annual W10m reduction of approximately 37% over highly urbanized areas in the PRD region relative to a 'no urban' case, similar to the -33% difference in mean daytime W10m between PRESENT and NOURB in the current study (Table 1). Using computational fluid dynamics simulations and detailed 3D building data reconstructed for the past, Peng et al. (2018) estimated a 50% weakening of wind speed in the lowest 25 m of the atmosphere over three highly urbanized study areas in Kowloon since 1964. With reference to Fig. 8a,b, the mean daytime W10m over the Kowloon peninsula decreased from 1–4 m/s in the PAST to 0.5–2 m/s in the PRESENT, corroborating the findings of Peng et al. (2018). Such agreements with previous findings, including some run at very fine resolutions, confirm the reliability of the simulations conducted in the current study.

The vertical structure of a coastal-urban boundary layer is relatively less studied because of its highly dynamic nature and difficulty in obtaining measurements for evaluation, especially in high-rise cities (Barlow, 2014). Wang et al. (2014) simulated a strong increase in summer PBL height of ~200 m in the day due to urbanization. Although not examined for all urban areas in D4, urban developments in Kowloon indeed lead to a deepening of the PBL on some days during the simulated period (Figs. 9 and A6). Melecio-Vázquez et al. (2018) investigated θ profiles in New York, USA. Two of their findings are similar to the current study: 1) The presence of a super-adiabatic layer in the lowest 250 m during the day in the highly urbanized areas as in Figs. 5c, 9b and A6b. 2) The fact that the urban boundary layer in the coastal city becomes slightly stable above ~500 m due to the formation of an internal boundary layer that is directly influenced by the urbanized land surface, as modelled over eastern Kowloon along the SE transect (Fig. A6b). This is also observed in the radiosounding at LT 8 on 21 May 2018, but not very well reproduced by the model (Fig. 5b). At LT 14, however, the boundary layer is well-mixed at KP (Fig. 5c). On the western Kowloon peninsula, Q_h is most likely stronger than for the site in New York. As a result, the stable layer above 500 m present at LT 8 becomes well-mixed by LT 14 whereas it is observed throughout the entire day in New York.

5.3. Urban heat island characteristics of Hong Kong

The UHI of Hong Kong has been quantified by many using the temperature difference between selected pairs of weather stations (e.g. Giridharan et al., 2005; Wu et al., 2009; Memon et al., 2011; Siu and Hart, 2013). However, owing to strong local influences by Hong Kong's heterogeneous land cover, complex topography, and rapid urbanization in neighbouring mainland cities, there has been no consensus on the representative rural station (Table 1 of Siu and Hart, 2013). With the help of numerical simulations, the UHI is objectively defined as the T2m difference in urban areas relative to NOURB in the current study. This approach is commonly used in modelling studies such as Gardes et al. (2020) for French cities and Tokairin et al. (2010) for the Asian megacity Jakarta. The mean daily and nocturnal UHI for the simulated heatwave in the PRESENT are both 0.5 K (Table 1). Although the UHI may have already been amplified during the simulated heatwave as in other cities (e.g. Basara et al., 2010; De Ridder et al., 2017; Rogers et al., 2019), the UHI of Hong Kong in the current study is quite small. Three possible reasons are discussed: 1) One of the main causes of UHI is the higher heat capacity of urban fabric compared to natural surfaces in rural areas. But, since large areas of sea with high heat capacity have been converted to land for urban development in Hong Kong, the mean UHI of the city is dampened, especially at night. 2) Seasonality is a major factor of UHI intensity. Previous studies revealed that the strongest UHI in Hong Kong occurs in winter, and the weakest in spring and summer (Wu et al., 2009; Memon et al., 2011). Analysing 20 years of temperature records at selected weather stations, Memon et al. (2011) reported a mean daily UHI of 0.4 K for May, which agrees well with the current study findings. 3) A positive relationship has been found between UHI intensity and the latitudinal variation in radiation balance and Q_f (Wienert and Kuttler, 2005). Hence, the ~2 K difference in nocturnal UHI during a heatwave in subtropical Hong Kong and temperate Paris (De Ridder et al., 2017) may in fact not be too surprising.

5.4. Extreme heat risk in Hong Kong

During the selected prolonged heatwave in May 2018, urban dwellers spend an alarmingly long duration – almost the entirety of the daylight hours – under SHS and VSHS (Table 1). Although the modelled daytime heat stress may have been exaggerated due to the overestimation of near-surface temperature in the last 5 days of the simulation period, the potential threats of heatwaves with increasing frequency, length, and severity under climate change to human health should not be overlooked. Without any adaptation, serious impacts on heatwave-related morbidity and excess mortality are expected in tropical/subtropical regions (Guo et al., 2018). It is therefore imperative to assess the extreme heat risk in Hong Kong and put in place appropriate mitigation strategies to reduce urban heat stress and the related health risks. Hua et al. (2021) mapped the spatiotemporal variability of extreme heat risk in Hong Kong based on the three components, namely hazard, exposure, and vulnerability, of Crichton's risk triangle (Crichton, 1999). Similar to the analysis in Section 4.4 of this paper, hazard is quantified by the number of HNHs (also very hot day hours in Hua et al., 2021) while exposure is quantified by the population density. The additional component of vulnerability is quantified by a series of demoesocioeconomic indicators. Planning districts with high heat risk largely match those identified in the current study (Fig. 11), with a few more in the north-eastern part of Kowloon (e.g. Wong Tai Sin and Choi Hung) where there is a high percentage of elderly and population with low education and income, as well as the district in the town centre of Shatin where many live in public rental housing and daytime heat stress is particularly high (Hua et al., 2021). The congested and poorly ventilated living environments in subdivided flats (common in 'Tong Lau') prevalent in older districts (e.g. MK, SSP, SW, WC, YMT) also add to the nighttime indoor overheating risks of urban residents (Board, 2020). The current study shows that shading by tall buildings is able to provide some urban heat stress relief in the day during a heatwave. Lau et al. (2016) presented similar findings but cautioned issues with air ventilation in a dense urban environment.

6. Conclusions and perspectives

In this study, the microclimatic effects of urban developments in Hong Kong have been investigated through a series of high-resolution (250 m) urban climate simulations using the mesoscale atmospheric model Meso-NH coupled to the multi-layer TEB. Detailed model input data have been constructed by a bottom-up GIS-based approach to represent the PAST (early 1960s), PRESENT (2018), and FUTURE (late 2040s) urban forms and functions of Hong Kong. To take into account the extreme climate conditions which are likely to occur more frequently in the future, a prolonged heatwave in May 2018 has been selected as the simulation period for all three urban datasets. Model output for the PRESENT has been evaluated against station surface observations and radiosoundings and a satisfactory performance has been achieved, allowing us to have confidence in the study findings.

The study highlights that the remarkable increases in urban extent and built-up density in Hong Kong from PAST to PRESENT/FUTURE have caused urban hot spots to expand and have altered the low-level wind field considerably. The strongest daytime UHI (compared to NOURB) is found to be caused by land reclamation, notably over the East Lantau artificial islands in the FUTURE. Warmer and drier conditions accompanied by less potential for ventilation are also expected for areas downwind of the artificial islands. The surface energy balance of Shatin new town no longer exhibits the characteristics of a suburban area as in the PAST and a strong reduction in daytime wind speed is observed due to the high-rise residential developments and the infilling of Shing Mun River which once served as an important air path. Moreover, changes in building architecture and cooling practices, exemplified by the evolution of the central business district from PAST to PRESENT, have resulted in large increases in anthropogenic and sensible heat fluxes, as well as the rapid release of heat stored in building materials in the evening. Besides modifying the surface meteorological variables and energy balance, urban development on the Kowloon peninsula has led to the formation of an unstable surface layer, a deepening of the planetary boundary layer, and an enhanced UHI circulation in the PRESENT simulation – effects that could not be verified regrettably due to the lack of data. Indeed, the marine-land transition and diurnal evolution of the urban boundary layer in a high-rise coastal city is a topic worthy of further investigation, should resource and techniques for obtaining representative measurements become available.

Study findings also show high risk of heat stress in all major urban areas of Hong Kong during the selected prolonged heatwave event. The amount of time during which urban dwellers are exposed to strong to very strong heat stress increases from PAST to FUTURE. Nighttime heat stress is of concern particularly in the densely populated, old residential areas of Kowloon. Building shading within compact urban settings may provide some relief to very strong heat stress in the day, but the intensifying nocturnal UHI and the potential issues on air ventilation should be noted. To mitigate the excess urban heat without compromising air ventilation in high-density Hong Kong, [Ng et al. \(2011\)](#) has recommended improvements in urban planning and design by creating air paths, introducing urban porosity, aligning street blocks with the prevailing wind direction etc.. Increasing urban greenery in the forms of grass surfaces, street trees, and pocket parks is another effective strategy to cool the urban environment, especially at night ([Ng et al., 2012](#); [Lin et al., 2017](#)). Upon understanding how the different urban development processes influence the urban climate of Hong Kong, further work is required to evaluate the effectiveness of various urban heat mitigation strategies and to explore their applicability and implementation in future (re)development plans.

Finally, since the current study relies on a single heatwave episode simulated for the different urban forms and functions, the climatic effects by the extremely hot and dry weather may have overshadowed those due to urbanization, resulting in diminished differences between the PAST, PRESENT, and FUTURE. Therefore, further work would benefit from examining a range of typical and extreme meteorological situations, and better still, to incorporate the projected future climate conditions.

CRedit authorship contribution statement

Yu Ting Kwok: Conceptualization, Methodology, Formal analysis, Investigation, Writing - original draft, Writing - review & editing, Visualization. **Robert Schoetter:** Conceptualization, Software, Investigation, Writing - original draft, Writing - review & editing, Funding acquisition. **Cécile de Munck:** Conceptualization, Writing - review & editing. **Kevin Ka-Lun Lau:** Resources, Writing - review & editing, Funding acquisition. **Man Sing Wong:** Resources. **Edward Ng:** Funding acquisition, Supervision.

Declaration of competing interest

The authors declare that they have no known competing financial interests or personal relationships that could have appeared to influence the work reported in this paper.

Acknowledgements

This work is supported by a grant from the PROCORE-France/Hong Kong Joint Research Scheme sponsored by the Research Grants Council and the Consulate General of France in Hong Kong (Reference No. F-CUHK403/18, 42552SL/F), as well as the Vice-Chancellor's Discretionary Fund of the Chinese University of Hong Kong. Radiosonde observations are obtained with the help of Mr. Wai King Wong from the Hong Kong Observatory. The authors would also like to thank Miss Tammy Lai for her photo in [Fig. 1b](#) and Miss Wang Ran for providing the historical LCZ map of the PRD region. Lastly, we acknowledge the support of the CUHK Central High Performance Computing Cluster, on which the computation in this work has been performed.

Appendix

Table A1
Prevalence of grid-dominant building archetypes in the PAST, PRESENT, and FUTURE within the domain of investigation.

Land use and building archetype	PAST		PRESENT		FUTURE	
	Count	%	Count	%	Count	%
Commercial						
Commercial skyscraper	–	–	40	0.7	80	1.3
Luxury hotel	–	–	11	0.2	11	0.2
Shopping mall	–	–	13	0.2	34	0.6
Old commercial building	–	–	7	0.1	2	0.0
Industrial						
Industrial building	135	7.4	198	3.5	178	3.0
Residential/mixed commercial-residential						
Public housing	146	8.0	294	5.2	343	5.7
Tong Lau	174	9.5	26	0.8	11	0.2
Private housing	–	–	154	2.7	119	2.0
Newer private housing	–	–	102	1.8	239	4.0
Modern private housing	–	–	27	0.5	37	0.6
Mid-rise/village house	629	34.3	766	13.6	805	13.4
Institutional, Governmental, Communal (GIC), transport, and others						
School	–	–	88	1.6	105	1.8
University/institution	–	–	75	1.3	74	1.2
Hospital	–	–	37	0.7	48	0.8
Other GIC	509	27.7	2453	43.7	2683	44.8
Transport facility	–	–	116	2.1	110	1.8
Historical building	–	–	14	0.2	12	0.2
Informal/rural infrastructure	243	13.2	1176	20.9	1102	18.4
Total grids with buildings	1836	100.0	5617	100.0	5993	100.0

The PAST lacks a full spectrum of archetypes due to insufficient information.

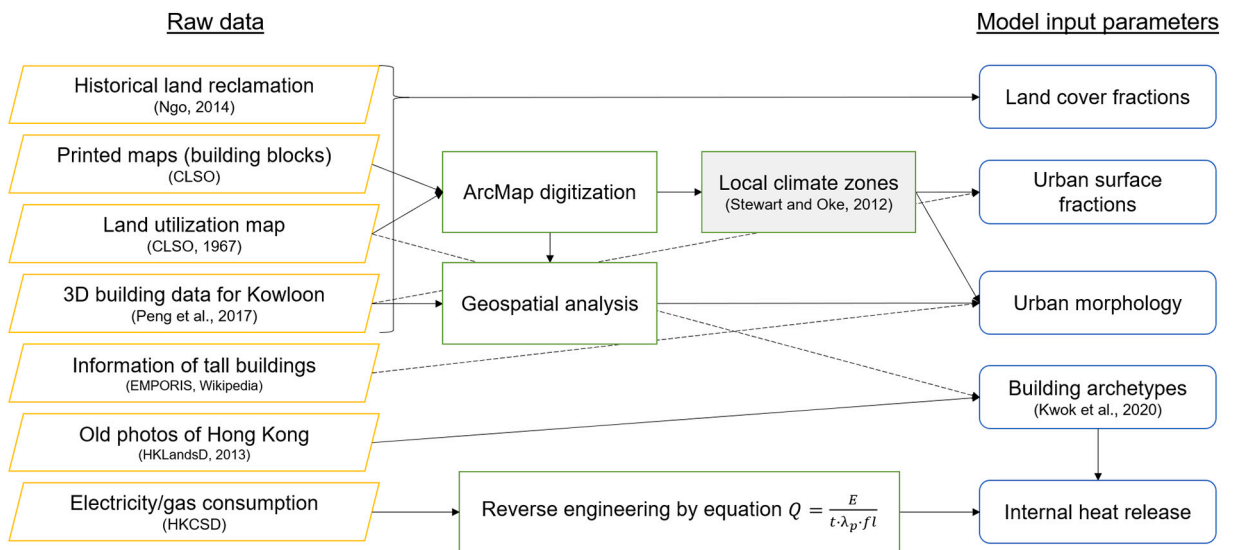


Fig. A1. Data and workflow to obtain model surface input parameters for the PAST. The local climate zone parameters (shaded box) are only used for major villages and squatter areas (Fig. A2). In the equation, Q is the internal heat release for domestic and commercial buildings in W/m^2 , E is the monthly domestic and commercial energy use in J , t is the number of seconds in May, λ_p is the total plan area of domestic and commercial buildings in m^2 , fl is the total number of floors in these buildings assuming a floor height of 3 m (Hong Kong Lands Department (HKLandsD) Survey and Mapping Office, 2020; Ngo, 2014; Stewart and Oke, 2012).

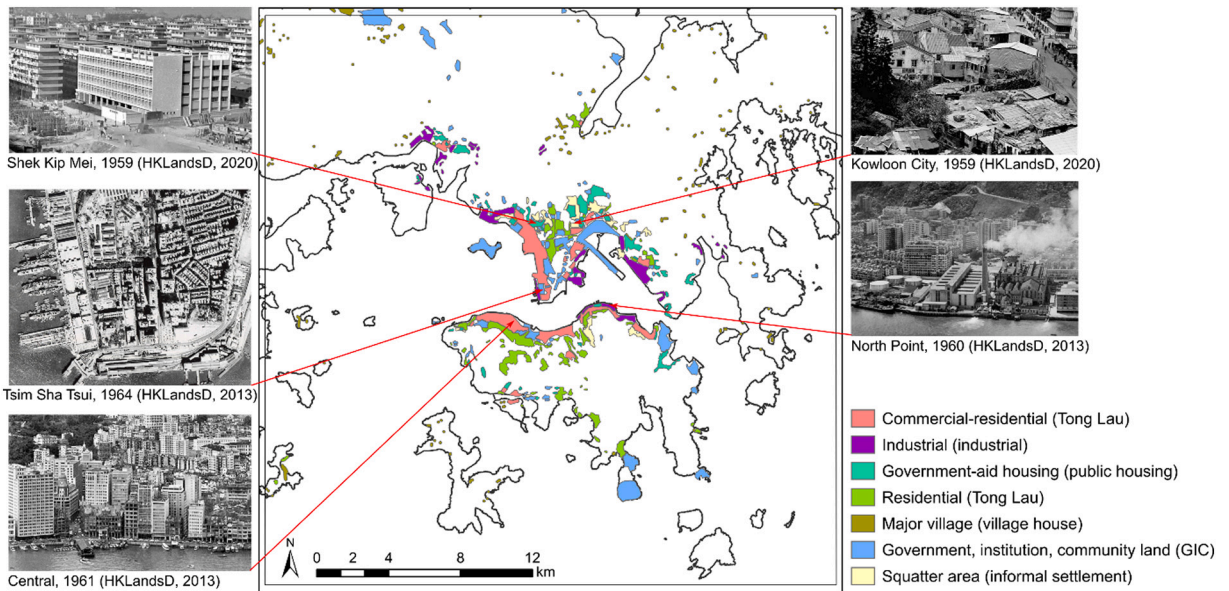


Fig. A2. Land use approximated from CLSO (1967) and reference photos for the different building archetypes in the PAST (Hong Kong Lands Department (HKLandsD) Survey and Mapping Office, 2020; Ngo, 2014; Stewart and Oke, 2012).

Table A2

Summary of new developments within the domain of investigation considered in the FUTURE.

Year	Study/project/report name	Classification	Timescale
2020	West Kowloon Cultural District (https://www.westkowloon.hk/en/the-district)	2c	Short
2020	MTR Shatin to Central Link (https://www.mtr-shatincentrallink.hk/en/construction/progress-update.html)	3c	Short
2019	Kai Tak Planning Review and Kai Tak Development (https://www.ktd.gov.hk/eng/overview.html)	2c	Short - medium
2019	Studies related to Artificial Islands in the Central Waters, Lantau Conservation Fund and Work Progress of the Sustainable Lantau Office, Legislative Council Paper No. CB(1)729/18-19(03)	1a	Medium - long
2018	Striving for Multi-pronged Land Supply - Report of the Task Force on Land Supply	0	Medium - long
2018	Planning and Design Study on the Redevelopment of Government Sites at Sai Yee Street and Mong Kok East Station – Feasibility Study	3c	Short
2017	Planning and Design Study on the Redevelopment of Queensway Plaza, Admiralty – Feasibility Study	3c	Medium
2016	Hong Kong 2030+ Towards a Planning Vision and Strategy Transcending 2030, Public Engagement & Preliminary Concepts for the East Lantau Metropolis	1a	Short - long
2016	Planning and Engineering Study for Re-planning of Tseung Kwan O Area 137 - Feasibility Study	2a	Short
2016	Energizing Kowloon East, Conceptual Master Plan 5.0	1b	Short -medium
2015	Draft Planning Brief for the “Comprehensive Development Area” Site in Diamond Hill	2b	Short - medium
2015	Urban Design Study for the Wan Chai North and North Point Harbourfront Areas - Feasibility Study	2c	Short
2014	Planning Study on Future Land Use at Anderson Road Quarry - Feasibility Study	2c	Short
2014	Planning Review on Development of Ex-Cha Kwo Ling Kaolin Mine Site	2c	Short
2014	Increasing Land Supply by Reclamation and Rock Cavern Development cum Public Engagement - Feasibility Study	0	Medium - long
2012	Planning and Engineering Study on Future Land Use at Ex-Lamma Quarry Area at Sok Kwu Wan, Lamma Island - Feasibility Study	2b	Short
2011	Urban Design Study for the New Central Harbourfront – Final report	2c	Short

The study classification includes information on the scale/nature of study (0 – review/exploratory study, 1 – city-wide/district-scale strategical framework, 2 – development areas, 3 – clustered/isolated development sites) and the level of detail available (a – design concept only, b – outline development plan with specification of land use and building height restrictions, c – site details on master layout plan). The development timescale is roughly defined as short-term (ongoing or to be realised within the next 3 years), medium-term (to be realised in the next 3–10 years), and long-term (to be realised in the next 10–30 years).

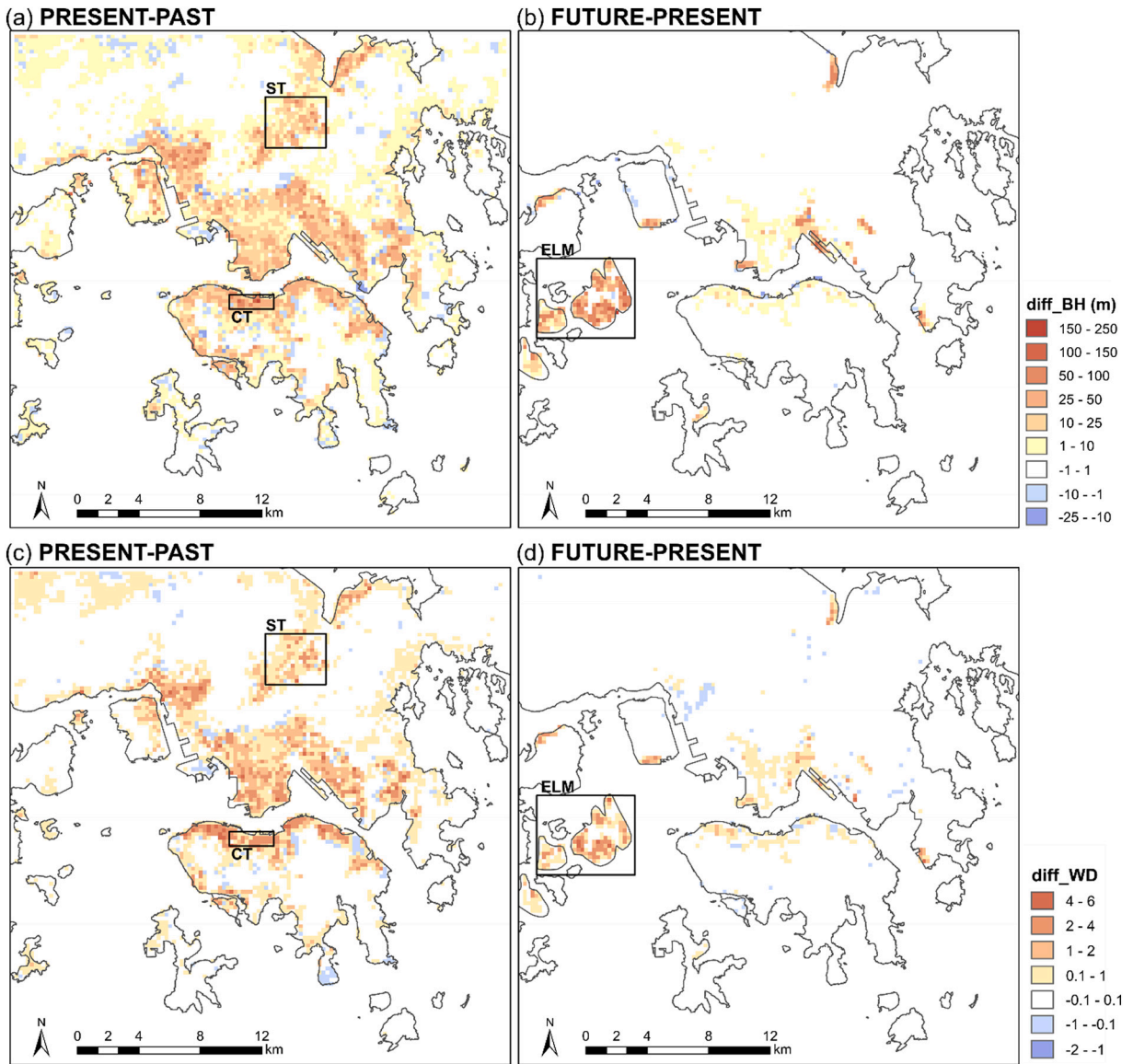


Fig. A3. Difference in building height and wall density for (a,c) PRESENT-PAST and (b,d) FUTURE-PRESENT within the domain of investigation. The selected subdomains for discussion in Section 5.1 are marked and labelled.

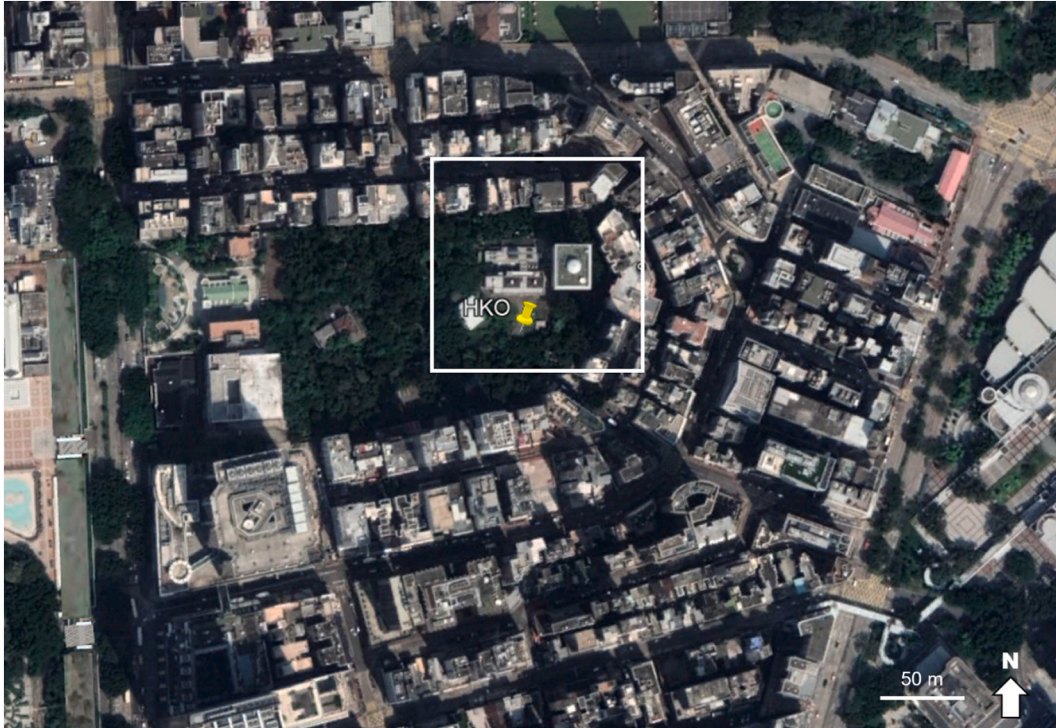


Fig. A4. Surrounding environment of the station HKO and the 125-m resolution model grid extent where the station is located (image source: Google Earth).

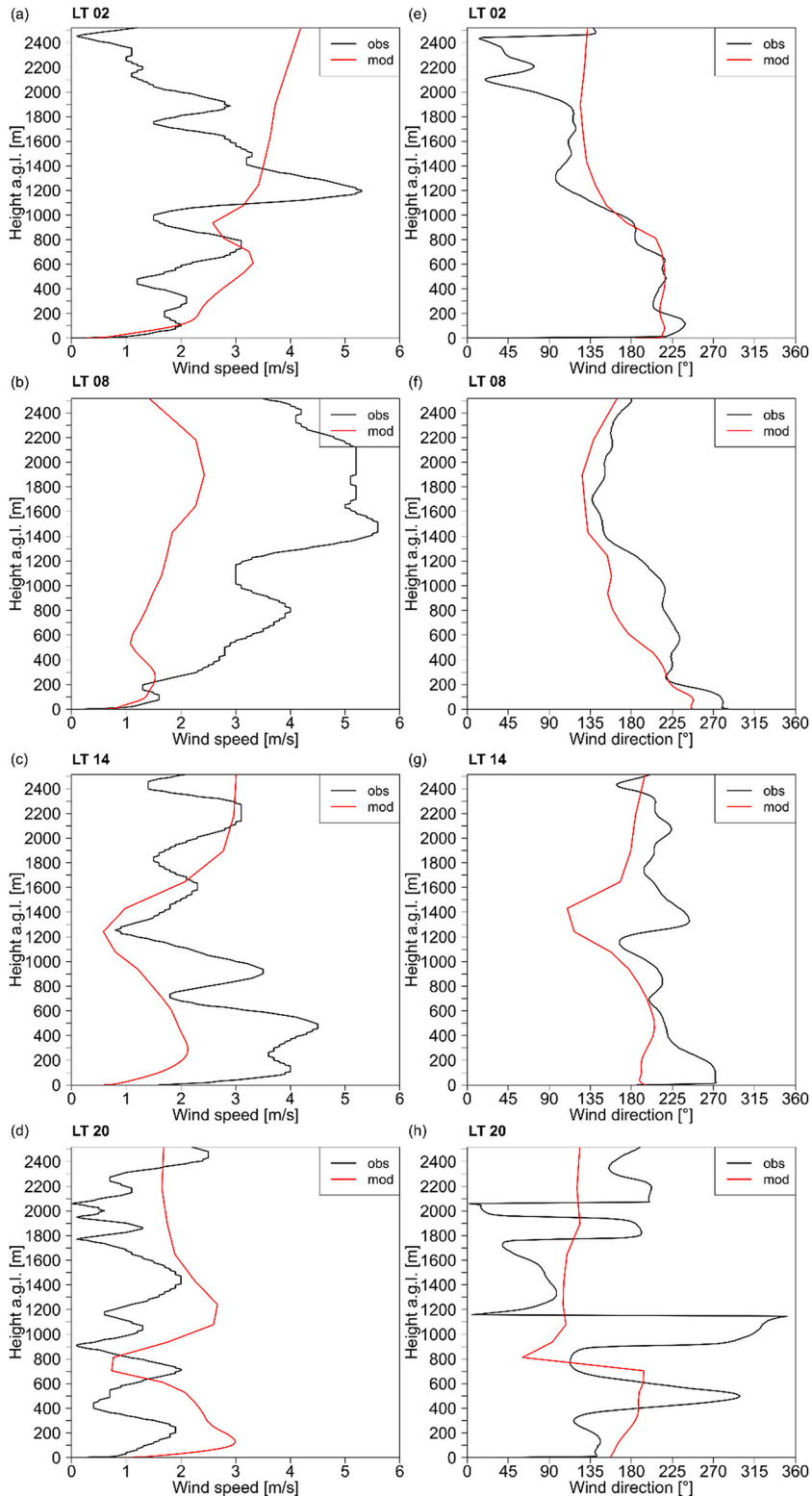


Fig. A5. Vertical profiles of the modelled (D5) and radiosonde observations at station KP of (a-d) wind speed and (e-h) wind direction at local time 02 (UTC 18 of the previous day), 08 (UTC 00), 14 (UTC 06), and 20 (UTC 12) on 21 May 2018 for the PRESENT.

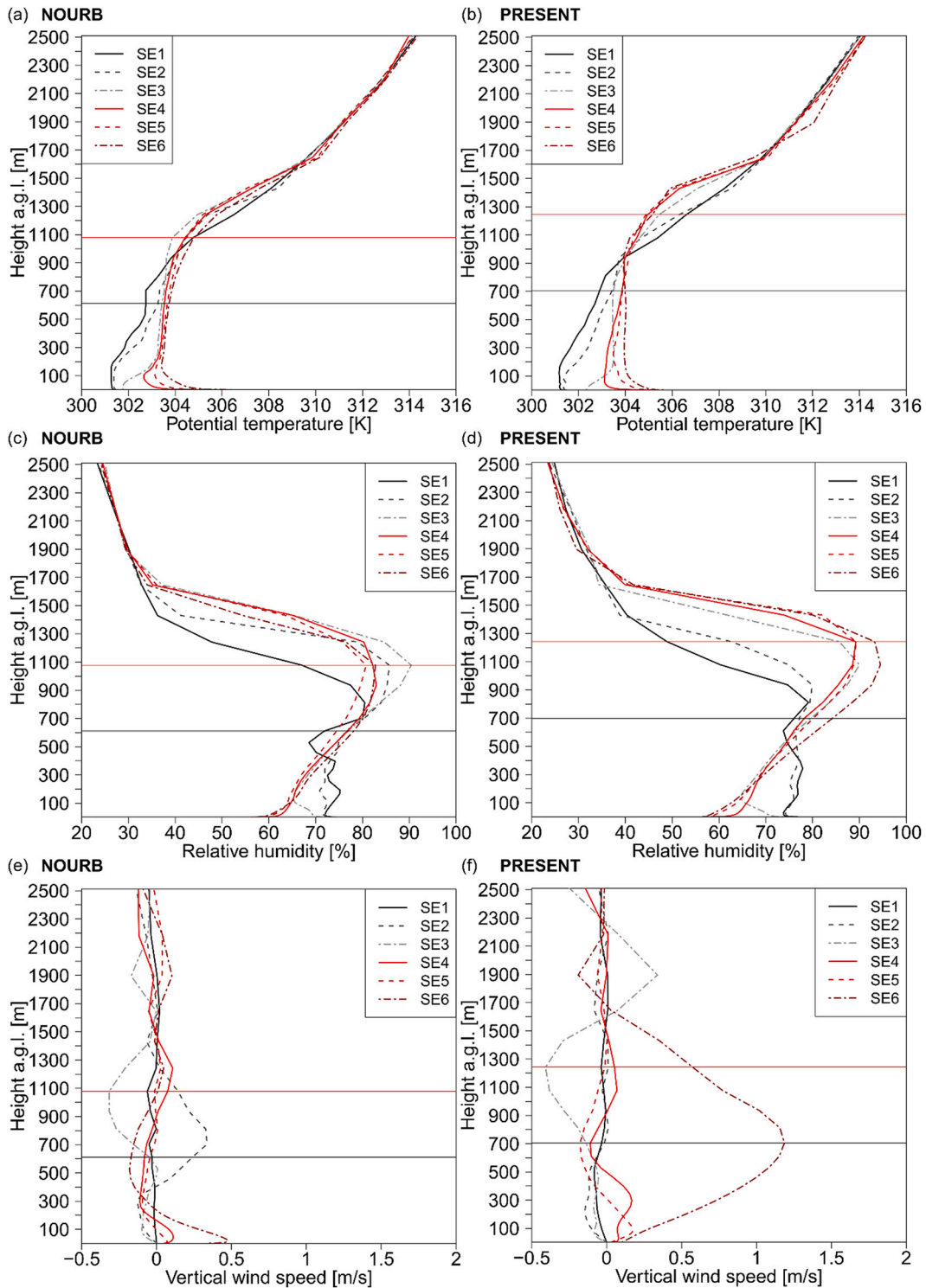


Fig. A6. Vertical profiles of (a,b) potential temperature, (c,d) relative humidity, and (e,f) vertical wind speed along the transect following the southwesterly wind flow (SE1–6) shown in Fig. 7 for NOURB and PRESENT on 21 May 2018 at LT 14. Vertical profiles over the sea and land are shown in black/grey and red, respectively. The planetary boundary layer depth of profiles 1 and 4 for both scenarios are estimated from potential temperature based on Sullivan et al., 1998. (For interpretation of the references to colour in this figure legend, the reader is referred to the web version of this article.)

References

- Artola, I., Rademakers, K., Williams, R., Yearwood, J., 2016. Boosting Building Renovation: What Potential and Value for Europe? Study for the iTRE Committee No. PE 587.326. Policy Department A: Economic and Scientific Policy, European Parliament, Brussels.
- Barlow, J.F., 2014. Progress in observing and modelling the urban boundary layer. *Urban Clim.* 10, 216–240.
- Basara, J.B., Basara, H.G., Illston, B.G., Crawford, K.C., 2010. The impact of the urban heat island during an intense heat wave in Oklahoma city. *Adv. Meteorol.* 2010. Article ID 230365.
- Błażejczyk, K., Bröde, P., Fiala, D., Havenith, G., Holmér, I., Jendritzky, G., et al., 2010. Principles of the new universal thermal climate index (UTCI) and its application to bioclimatic research in european scale. *Misc. Geograph.* 14 (1), 91–102.
- Błażejczyk, K., Jendritzky, G., Bröde, P., Fiala, D., Havenith, G., Epstein, Y., et al., 2013. An introduction to the universal thermal climate index (UTCI). *Geogr. Pol.* 86 (1), 5–10.
- Board, J., 2020. Hot in the city: Rising night temperatures a potentially major health issue in Asian metropolises. *Channel News Asia*, 13 Sep. <https://www.channelnewsasia.com/news/asia/urban-heat-island-asia-bangkok-singapore-climate-change-health-13098858>.
- Bueno, B., Pigeon, G., Norford, L.K., Zibouche, K., Marchadier, C., 2012. Development and evaluation of a building energy model integrated in the TEB scheme. *Geosci. Model Dev.* 5, 433–448.
- Cai, M., Ren, C., Xu, Y., Dai, W., Wang, X.M., 2016. Local climate zone study for sustainable megacities development by using improved WUDAPT methodology—a case study in Guangzhou. *Procedia Environ. Sci.* 36, 82–89.
- Champeaux, J., Masson, V., Chauvin, F., 2005. ECOCLIMAP: a global database of land surface parameters at 1 km resolution. *Meteorol. Appl.: J. Forecast. Pract. Appl. Train. Tech. Model.* 12 (1), 29–32.
- Chan, H., Kok, M., Lee, T., 2012. Temperature trends in Hong Kong from a seasonal perspective. *Clim. Res.* 55 (1), 53–63.
- Ching, J., Mills, G., Bechtel, B., See, L., Feddema, J., Wang, X., et al., 2018. World urban database and access portal tools (WUDAPT), an urban weather, climate and environmental modeling infrastructure for the anthropocene. *Bull. Am. Meteorol. Soc.* 2018.
- Crichton, D., 1999. The risk triangle. *Nat. Disaster Manag.* 102 (3).
- Crown Land and Survey Office (CLSO) Colony Outline Planning Team, 1967. Land Utilization in Hong Kong as at 31st March 1966. The Government Printer, Hong Kong.
- De Ridder, K., Maiheu, B., Lauwaet, D., Daglis, I.A., Keramitsoglou, I., Kourtidis, K., et al., 2017. Urban heat island intensification during hot spells—the case of Paris during the summer of 2003. *Urban Sci.* 1 (1), 3.
- Development Bureau (HKDB), & Planning Department (HKPLand), 2016. Hong Kong 2030+ Towards a Planning Vision and Strategy Transcending 2030 - Public Engagement.
- Emporis, 2020. Hong Kong Buildings. Retrieved 7/30, 2020, from. <https://www.emporis.com/city/101300/hong-kong-china>.
- Environment Bureau (HKEB), 2015. Hong Kong Climate Change Report 2015. Environment Bureau, Hong Kong.
- Gardes, T., Schoetter, R., Hidalgo, J., Long, N., Marquès, E., Masson, V., 2020. Statistical prediction of the nocturnal urban heat island intensity based on urban morphology and geographical factors—an investigation based on numerical model results for a large ensemble of French cities. *Sci. Total Environ.* 139253.
- Ginn, W., Lee, T., Chan, K., 2010. Past and future changes in the climate of Hong Kong. *J. Meteorol. Res.* 24 (2), 163–175.
- Giridharan, R., Lau, S., Ganesan, S., 2005. Nocturnal heat island effect in urban residential developments of Hong Kong. *Energy Build.* 37 (9), 964–971.
- Goggins, W.B., Chan, E.Y., Ng, E., Ren, C., Chen, L., 2012. Effect modification of the association between short-term meteorological factors and mortality by urban heat islands in Hong Kong. *PLoS One* 7 (6), e38551.
- Guo, Y., Gasparrini, A., Li, S., Sera, F., Vicedo-Cabrera, A.M., De Sousa Zanotti Stagliorio Coelho, M., et al., 2018. Quantifying excess deaths related to heatwaves under climate change scenarios: a multicountry time series modelling study. *PLoS Med.* 15 (7), e1002629.
- Hills, P., Yeh, A.G.O., 1983. New town developments in Hong Kong. *Built Environ.* (1978-) 266–277.
- Ho, H.C., Lau, K.K., Ren, C., Ng, E., 2017. Characterizing prolonged heat effects on mortality in a sub-tropical high-density city, Hong Kong. *Int. J. Biometeorol.* 61 (11), 1935–1944.
- Hong Kong Census and Statistics Department (HKCSD), 1969. Hong Kong Statistics: 1947–1967 Census & Statistics Department, Hong Kong.
- Hong Kong Census and Statistics Department (HKCSD), 2018. Population By-Census Results. Retrieved 11/26, 2020, from. <https://www.bycensus2016.gov.hk/en/bc-index.html>.
- Hong Kong Lands Department (HKLandsD) Survey and Mapping Office, 2013. Hong Kong Now and Then: A Collection of Hong Kong Aerial Photos 今日昔日香港: 香港航空照片集. Hong Kong Lands Department Survey and Mapping Office, Hong Kong.
- Hong Kong Lands Department (HKLandsD) Survey and Mapping Office, 2020. Old Photos of Hong Kong. Retrieved 9/28, 2020, from. <https://data.gov.hk/en-data/dataset/hk-landsd-openmap-old-photos-of-hong-kong>.
- Hong Kong Planning Department (HKPLand), 2020. Land Utilization in Hong Kong 2019. Retrieved 11/25, 2020, from. https://www.pland.gov.hk/pland_en/info_serv/statistic/landu.html.
- Hua, J., Zhang, X., Ren, C., Shi, Y., Lee, T., 2021. Spatiotemporal assessment of extreme heat risk for high-density cities: A case study of Hong Kong from 2006 to 2016. *Sustain. Cities Soc.* 64, 102507.
- Kwok, Y.T., Ng, E., 2021. Trends, topics, and lessons learnt from real case studies using mesoscale atmospheric models for urban climate applications in 2000–2019. *Urban Clim.* 31, 100785.
- Kwok, Y.T., Schoetter, R., Lau, K.K., Hidalgo, J., Ren, C., Pigeon, G., et al., 2019. How well does the local climate zone scheme discern the thermal environment of Toulouse (France)? An analysis using numerical simulation data. *Int. J. Climatol.* 39 (14), 5292–5315.
- Kwok, Y.T., De Munck, C., Schoetter, R., Ren, C., Lau, K.K., 2020. Refined dataset to describe the complex urban environment of Hong Kong for urban climate modelling studies at the mesoscale. *Theor. Appl. Climatol.* 142, 129–150.
- Laaidi, K., Zeghnoun, A., Dousset, B., Bretin, P., Vandentorren, S., Giraudet, E., et al., 2012. The impact of heat islands on mortality in Paris during the august 2003 heat wave. *Environ. Health Perspect.* 120 (2), 254–259.
- Lac, C., Chaboureaud, J., Masson, V., Pinty, J., Tulet, P., Escobar, J., et al., 2018. Overview of the meso-NH model version 5.4 and its applications. *Geosci. Model Dev.* 11, 1929–1969.
- Lau, K.L., Ng, E., 2013. An investigation of urbanization effect on urban and rural Hong Kong using a 40-year extended temperature record. *Landsc. Urban Plan.* 114, 42–52.
- Lau, K.K., Ren, C., Ho, J., Ng, E., 2016. Numerical modelling of mean radiant temperature in high-density sub-tropical urban environment. *Energy Build.* 114, 80–86.
- Lee, T.C., 2018. Will 2018 Be as Dry as 1963?, 2020, from. <https://www.hko.gov.hk/en/Observatorys-Blog/101818/Will-2018-be-as-dry-as-1963>.
- Lee, K., Chan, Y., Lee, T., Goggins, W.B., Chan, E.Y., 2016. The development of the Hong Kong heat index for enhancing the heat stress information service of the Hong Kong observatory. *Int. J. Biometeorol.* 60 (7), 1029–1039.
- Lin, W., Sui, C., Yang, L., Wang, X., Deng, R., Fan, S., et al., 2007. A numerical study of the influence of urban expansion on monthly climate in dry autumn over the pearl river delta, China. *Theor. Appl. Climatol.* 89 (1–2), 63–72.
- Lin, W., Zhang, L., Du, D., Yang, L., Lin, H., Zhang, Y., et al., 2009. Quantification of land use/land cover changes in pearl river delta and its impact on regional climate in summer using numerical modeling. *Reg. Environ. Chang.* 9 (2), 75–82.
- Lin, P., Lau, S.S.Y., Qin, H., Gou, Z., 2017. Effects of urban planning indicators on urban heat island: a case study of pocket parks in high-rise high-density environment. *Landsc. Urban Plan.* 168, 48–60.
- Lowry, W.P., 1977. Empirical estimation of urban effects on climate: a problem analysis. *J. Appl. Meteorol.* 16 (2), 129–135.
- Luo, M., Lau, N., 2017. Heat waves in southern China: synoptic behavior, long-term change, and urbanization effects. *J. Clim.* 30 (2), 703–720.
- Masson, V., 2000. A physically-based scheme for the urban energy budget in atmospheric models. *Bound.-Layer Meteorol.* 94 (3), 357–397.

- Masson, V., Le Moigne, P., Martin, E., Faroux, S., Alias, A., Alkama, R., et al., 2013. The SURFEXv7. 2 land and ocean surface platform for coupled or offline simulation of earth surface variables and fluxes. *Geosci. Model Dev.* 6, 929–960.
- Masson, V., Heldens, W., Bocher, E., Bonhomme, M., Bucher, B., Burmeister, C., et al., 2020. City-descriptive input data for urban climate models: model requirements, data sources and challenges. *Urban Clim.* 31, 100536.
- Melecio-Vázquez, D., Ramamurthy, P., Arend, M., González-Cruz, J.E., 2018. Thermal structure of a coastal–urban boundary layer. *Bound.-Layer Meteorol.* 169 (1), 151–161.
- Memon, R.A., Leung, D.Y., Liu, C., Leung, M.K., 2011. Urban heat island and its effect on the cooling and heating demands in urban and suburban areas of Hong Kong. *Theor. Appl. Climatol.* 103 (3–4), 441–450.
- Morakinyo, T.E., Ren, C., Shi, Y., Lau, K.K., Tong, H., Choy, C., et al., 2019. Estimates of the impact of extreme heat events on cooling energy demand in Hong Kong. *Renew. Energy* 142, 73–84.
- Ng, E., Yuan, C., Chen, L., Ren, C., Fung, J.C., 2011. Improving the wind environment in high-density cities by understanding urban morphology and surface roughness: a study in Hong Kong. *Landsc. Urban Plan.* 101 (1), 59–74.
- Ng, E., Chen, L., Wang, Y., Yuan, C., 2012. A study on the cooling effects of greening in a high-density city: an experience from Hong Kong. *Build. Environ.* 47, 256–271.
- Ngo, V., 2014. Mapping the History of Land Reclamation in Hong Kong. Retrieved 07/30, 2020, from <http://oldhkphoto.com/coast/>.
- Noilhan, J., Planton, S., 1989. A simple parameterization of land surface processes for meteorological models. *Mon. Weather Rev.* 117 (3), 536–549.
- Oke, T.R., 2006. Towards better scientific communication in urban climate. *Theor. Appl. Climatol.* 84 (1–3), 179–190.
- Peng, F., Wong, M.S., Ho, H.C., Nichol, J., Chan, P.W., 2017. Reconstruction of historical datasets for analyzing spatiotemporal influence of built environment on urban microclimates across a compact city. *Build. Environ.* 123, 649–660.
- Peng, L., Liu, J., Wang, Y., Chan, P., Lee, T., Peng, F., et al., 2018. Wind weakening in a dense high-rise city due to over nearly five decades of urbanization. *Build. Environ.* 138, 207–220.
- Pigeon, G., Zibouche, K., Bueno, B., Le Bras, J., Masson, V., 2014. Improving the capabilities of the town energy balance model with up-to-date building energy simulation algorithms: an application to a set of representative buildings in Paris. *Energy Build.* 76, 1–14.
- Planning Department (HKPlanD), 2012. Urban Climatic Map and Standards for Wind Environment - Feasibility Study No. Final Report.
- Rogers, C.D., Gallant, A.J., Tapper, N.J., 2019. Is the urban heat island exacerbated during heatwaves in southern Australian cities? *Theor. Appl. Climatol.* 137 (1–2), 441–457.
- Salgado, R., Le Moigne, P., 2010. Coupling of the FLake model to the SURFEX externalized surface model. *Boreal Environ. Res.* 15, 231–244.
- Schoetter, R., Kwok, Y.T., de Munck, C., Lau, K.K.L., Wong, W.K., Masson, V., 2020. Multi-layer coupling between SURFEX-TEB-V9.0 and meso-NH-v5.3 for modelling the urban climate of high-rise cities. *Geosci. Model Dev.* 13, 5609–5643.
- Shelton, B., Karakiewicz, J., Kvan, T., 2011. *The Making of Hong Kong: From Vertical to Volumetric*. Routledge, New York.
- Shi, Y., Ren, C., Cai, M., Lau, K.K., Lee, T., Wong, W., 2019. Assessing spatial variability of extreme hot weather conditions in Hong Kong: a land use regression approach. *Environ. Res.* 171, 403–415.
- Shun, C., Lee, S., 2017. The science of climate change and its relevance to Hong Kong. *Bienn. J. Hong Kong Elect. Contract. Assoc. Limit* 18, 84–90.
- Siu, L.W., Hart, M.A., 2013. Quantifying urban heat island intensity in Hong Kong SAR, China. *Environ. Monit. Assess.* 185 (5), 4383–4398.
- Smart, A., 2006. *The Shek Kip Mei myth: Squatters, Fires and Colonial Rule in Hong Kong, 1950–1963*. Hong Kong University Press.
- So, K., Guo, H., Li, Y., 2007. Long-term variation of PM_{2.5} levels and composition at rural, urban, and roadside sites in Hong Kong: increasing impact of regional air pollution. *Atmos. Environ.* 41 (40), 9427–9434.
- Stewart, I.D., Oke, T.R., 2012. Local climate zones for urban temperature studies. *Bull. Am. Meteorol. Soc.* 93 (12), 1879–1900.
- Sullivan, P.P., Moeng, C., Stevens, B., Lenschow, D.H., Mayor, S.D., 1998. Structure of the entrainment zone capping the convective atmospheric boundary layer. *J. Atmos. Sci.* 55 (19), 3042–3064.
- The Hong Kong Special Administrative Region (HKSAR), 2018. The Chief Executive's 2018 Policy Address. Retrieved 10/23, 2018, from <https://www.policyaddress.gov.hk/2018/eng/policy.html>.
- Tokairin, T., Sofyan, A., Kitada, T., 2010. Effect of land use changes on local meteorological conditions in Jakarta, Indonesia: toward the evaluation of the thermal environment of megacities in asia. *Int. J. Climatol.* 30 (13), 1931–1941.
- Town Planning Board (TPB), 2020. Statutory Planning Portal 2. Retrieved 2/25, 2020, from <https://www2.ozp.tpb.gov.hk/gos/>.
- Tse, J.W.P., Yeung, P.S., Fung, J.C., Ren, C., Wang, R., Wong, M.M., et al., 2018. Investigation of the meteorological effects of urbanization in recent decades: a case study of major cities in pearl river delta. *Urban Clim.* 26, 174–187.
- Urban Renewal Authority (URA), 2020. Explore Our Projects. Retrieved 2/20, 2020, from <https://www.ura.org.hk/en/project/redevelopment>.
- Volldoire, A., Decharme, B., Pianezze, J., Lebeaupin Brossier, C., Sevault, F., Seyfried, L., et al., 2017. SURFEX v8. 0 interface with OASIS3-MCT to couple atmosphere with hydrology, ocean, waves and sea-ice models, from coastal to global scales. *Geosci. Model Dev.* 10 (11), 4207–4227.
- Wai, C., 2012. Energizing Kowloon East. Development Bureau, HKSAR Government.
- Wang, X., Liao, J., Zhang, J., Shen, C., Chen, W., Xia, B., et al., 2014. A numeric study of regional climate change induced by urban expansion in the pearl river delta, China. *J. Appl. Meteorol. Climatol.* 53 (2), 346–362.
- Wang, D., Lau, K.K., Ren, C., Goggins, W.B.I., Shi, Y., Ho, H.C., et al., 2019a. The impact of extremely hot weather events on all-cause mortality in a highly urbanized and densely populated subtropical city: a 10-year time-series study (2006–2015). *Sci. Total Environ.* 690, 923–931.
- Wang, R., Cai, M., Ren, C., Bechtel, B., Xu, Y., Ng, E., 2019b. Detecting multi-temporal land cover change and land surface temperature in pearl river delta by adopting local climate zone. *Urban Clim.* 28, 100455.
- Wang, Y., Chan, A., Lau, G.N., Li, Q., Yang, Y., Yim, S.H.L., 2019c. Effects of urbanization and global climate change on regional climate in the pearl river delta and thermal comfort implications. *Int. J. Climatol.* 39 (6), 2984–2997.
- Wienert, U., Kuttler, W., 2005. The dependence of the urban heat island intensity on latitude—a statistical approach. *Meteorol. Z.* 14 (5), 677–686.
- Wong, M., Mok, H., Lee, T., 2011. Observed changes in extreme weather indices in Hong Kong. *Int. J. Climatol.* 31 (15), 2300–2311.
- Wong, M.S., Yang, J., Nichol, J., Weng, Q., Menenti, M., Chan, P.W., 2015. Modeling of anthropogenic heat flux using HJ-1B Chinese small satellite image: a study of heterogeneous urbanized areas in Hong Kong. *IEEE Geosci. Remote Sens. Lett.* 12 (7), 1466–1470.
- Wu, M.C., Leung, Y.K., Lui, W.M., Lee, T.C., 2009. 香港城市与郊区气候差异分析 a study on the difference between urban and rural climate in Hong Kong (with English abstract). *气象* 35 (2), 71–79.
- Wu, M., Luo, Y., Chen, F., Wong, W.K., 2019. Observed link of extreme hourly precipitation changes to urbanization over coastal South China. *J. Appl. Meteorol. Climatol.* 58 (8), 1799–1819.
- Yeung, P.S., Fung, J.C., Ren, C., Xu, Y., Huang, K., Leng, J., et al., 2020. Investigating future Urbanization's impact on local climate under different climate change scenarios in MEGA-urban regions: a case study of the pearl river delta, China. *Atmosphere* 11 (7), 771.
- Zhang, X.Q., 2000. High-rise and high-density compact urban form: the development of Hong Kong. *Compact Cities: Sustain. Urban Forms Dev. Countries* 245, 254.
- Zou, H., 2013. A history of the evolution of building control in Hong Kong (1841–1997). *Appl. Mech. Mater.* 357, 257–260.